https://doi.org/10.5194/egusphere-2026-1653
Preprint. Discussion started: 26 March 2026

An Automated Method for Polynya Detection Using a Geomorphon Algorithm

Mia Hurst[1], Lars Boehme[1]

[1]Scottish Oceans Institute, University of St Andrews, St Andrews, KY16 8LB, United Kingdom

Correspondence to: Mia Hurst (mh326@st-andrews.ac.uk)

Abstract. Polynyas, persistent areas of open water within sea ice, are critical features of polar marine systems, facilitating ocean-atmosphere heat exchange, deep water formation, nutrient cycling, and biological productivity. However, current remote detection methods, typically based on sea ice concentration thresholds, often struggle to capture the complex morphology of polynyas, especially fine-scale coastal features, and can be time-consuming to use and inconsistent across spatial scales. This study presents a novel application of a geomorphon pattern recognition algorithm, originally developed for terrestrial landform classification, to automate polynya detection using sea ice concentration data. Focusing on two key Southern Ocean regions, the Weddell and Amundsen Seas, we assess the algorithm's performance through a comprehensive sensitivity analysis, involving 96 and 144 parameter combinations respectively, and compare the results to polynyas identified using a traditional sea ice concentration threshold-based method. By identifying morphological analogues, such as depressions and valleys in sea ice concentration data, the geomorphon method effectively captures spatial patterns and areal extents of polynyas, closely aligning with results from traditional threshold-based approaches and literature reports. The method's scalability and self-adaptive lookup distance allows detection of both large-scale open water and small coastal polynyas. Application of analytically rescaled parameters to an independent passive microwave sea ice concentration dataset further demonstrated transferability across datasets and spatial resolutions without additional optimisation. Critically, its automated nature enables rapid processing of time series data, up to two orders of magnitude faster than traditional methods, making it well-suited for investigating long-term polynya dynamics. By enabling consistent detection across large datasets, the method provides a framework to support investigations into climate-sensitive ocean processes, including air-sea fluxes, water mass formation, carbon cycling, and ecosystem dynamics in polar regions.

1 Introduction

1.1 Sea Ice and Polynya Dynamics

Sea ice is a defining feature of the polar regions and plays a large role in driving ocean circulation and global climate patterns by helping to regulate exchanges of heat, moisture, and salinity at the ocean-atmosphere boundary (Houghton et al., 1996). When sea ice forms brine rejection occurs, where the salt in seawater is pushed out of the forming ice crystals, which increases

https://doi.org/10.5194/egusphere-2026-1653
Preprint. Discussion started: 26 March 2026

the salinity of the surface waters below the ice (Wakatsuchi and Ono, 1983; Nomura et al., 2021). The dense, cold, and saline water masses which are produced sink, and contribute to the formation of bottom water, which helps to sustain global overturning circulation (Comiso and Gordon, 1998; Ohshima et al., 2016). Moreover, by providing a physical barrier between the ocean and atmosphere, sea ice insulates the relatively warm ocean waters from the cold polar atmosphere, preventing the exchange of heat and water vapour (Landrum and Holland, 2022). This insulating effect helps to regulate surface temperatures and influences atmospheric circulation by modifying heat fluxes and pressure gradients (Walsh and Johnson 1979; Budikova, 2009).

Continuous sea ice can be interspersed with areas of open water, forming regions of direct interaction between the ocean and the atmosphere. These areas can be narrow linear fractures in sea ice, known as leads, or large semi-persistent areas of open water, called polynyas. Polynyas are very important oceanographic features, acting as sites of strong ocean-to-atmosphere heat and moisture transfers (Morales Maqueda et al., 2004; Barber and Massom, 2007; Yager et al., 2016). These transfers cause the air column above and downwind of the polynya to rapidly warm, modifying local atmospheric and oceanic conditions (Alam and Curry, 1995; Gallée, 1997). Additionally, polynyas act as important carbon sinks, as their surface waters sequester vast amounts of atmospheric CO_2 (Hoppema and Anderson, 2007). When these processes are combined across multiple polynyas, their effect can be globally significant. For example, over the entire Arctic Ocean up to 50% of the total atmosphere-ocean heat and CO_2 exchanged in winter occurs through polynyas and leads (Maykut, 1982; Else et al., 2013). Antarctic polynyas are also considered a significant carbon sink, with rates of CO_2 fixation frequently exceeding 2 g C m^{-2} d^{-1} (Louanchi et al., 1999; Arrigo and van Dijken, 2003).

Polynyas can range between 10 to 10^5 km^2 in size and often occur at specific geographical locations and phases of the year (Barber et al., 2001). Polynyas can be classified as either open-ocean or coastal, and can have different formation mechanisms (Gordon and Comiso, 1988). Open-ocean polynyas are typically thermally driven, occurring in regions of upwelling where warm buoyant water rises through the water column and melts sea ice, generating open water areas (Martinson, 1991; Zheng et al., 2021). In contrast, coastal polynyas are typically formed when strong offshore winds advect sea ice away from the coast, creating areas of open water (Bromwich and Kurtz, 1984; Morales Maqueda et al., 2004; Bennett et al., 2024).

Whilst both polynya types are important for ocean-to-atmosphere exchanges, their different formation processes mean that they also perform unique roles. Open-ocean polynyas are crucial for large scale circulation, acting as sites of deep convection that influence global thermohaline circulation and facilitate nutrient upwelling (Melling et al., 2001; Cheon and Gordon, 2019). A prominent example is the Weddell Sea Polynya, which first gained scientific attention in the 1970s when it opened for several consecutive winters within the dense pack ice of the southern Weddell Sea (Carsey, 1980). Its re-emergence in the 2010s has renewed scientific interest in its role in deep ocean convection, as it exposes relatively warm ocean to the atmosphere, promoting intense heat loss and vertical mixing (Mchedlishvili et al., 2022). The Weddell Sea Polynya provides

https://doi.org/10.5194/egusphere-2026-1653
Preprint. Discussion started: 26 March 2026

a rare window into processes that influence deep water formation and global thermohaline circulation, making it an important system for both climate and oceanographic studies (Cheon and Gordon, 2019). In comparison, coastal polynyas play a primary role in shaping ecosystem dynamics, local ice production and the creation of dense, saline bottom water (Comiso and Gordon, 1998; Kimura and Wakatsuchi, 2004; Arrigo and van Dijken, 2003). The ecological role which coastal polynyas perform is incredibly important in supporting high-latitude food webs. During summer months, the surface area of open water in coastal polynyas increases, allowing more light to penetrate the ocean and stimulate photosynthesis of phytoplankton (Dennett et al., 2001; Jena and Pillai, 2020). The large phytoplankton blooms that develop form the base of an entire ecosystem, and as a result coastal polynyas become critical habitats for a wide range of benthic and higher trophic level organisms (Gilchrist and Robertson, 2000; Labrousse et al., 2018). Coastal polynyas found in the Amundsen Sea are some of the most biologically productive polynyas in the Southern Ocean, forming along the coast of West Antarctica (Arrigo and van Dijken, 2003). Their persistence is influenced by offshore winds which help maintain areas of open water (Macdonald et al., 2023). The region has been identified as a hotspot for both high ice production and intense summertime phytoplankton blooms, linking it to key processes in dense water formation, biogeochemical cycling, and ecosystem support in the Amundsen Sea (Arrigo et al., 2012; Macdonald et al., 2023).

Although polynyas are commonly defined as areas of open water or thin sea ice surrounded by thicker sea ice, there is no single, universally accepted definition. Differences in the spatial and temporal criteria used across studies can significantly affect reported polynya characteristics. Most detection methods apply a sea ice concentration threshold, which can range between 20% and 80%, to distinguish open water from consolidated ice (Massom et al., 1998; Kern et al., 2007; Mohrmann et al., 2021). However, this value is somewhat arbitrary and can vary with the sensor, retrieval algorithm, and region. Persistence criteria also differ, with some studies requiring openings to remain for certain periods of time to classify open water regions as polynyas (Arrigo and van Dijken 2003). Size thresholds are rarely used to define polynyas within detection methods, typically due to the spatial resolution constraints of available data sources. However, polynyas have been reported to range in size from a few square kilometres to over 10^5 km² (Barber et al., 2001; Arrigo and van Dijken, 2003). In addition, polynyas can also be further categorised as open-ocean or coastal polynyas meaning that their geographical and spatial scale can differ substantially. This diversity in polynya characteristics highlights the importance of clearly defining what constitutes a polynya when developing or applying a detection technique.

1.2 Data Sources and Limitations

The ability to detect polynyas in observational satellite data and ocean reanalysis products is essential in improving our understanding of polynya dynamics. This is especially significant when we consider that their regionally and globally important roles are likely to be impacted by the effects of climate change, which will undoubtedly impact the extent and thickness of sea ice (Kim et al., 2023). Lack of in-situ data and observations of polynyas is often due to their remote locations

https://doi.org/10.5194/egusphere-2026-1653
Preprint. Discussion started: 26 March 2026

in harsh environments, which make them challenging to access (Ohshima et al., 2016). Despite this, a range of different data sources have been employed to study polynyas, each with their own strengths and limitations, making them more suitable for some applications than others. Satellite remote sensing has been used in the majority of studies researching polynya inter-annual dynamics, monitoring sea ice concentration and thickness (Paul et al., 2015; Jena and Pillai, 2020). These products are particularly valuable for confirming the presence or absence of polynyas in specific regions and months, and have supported many case studies of polynya variability (Zhou et al., 2023). However, even these technological advancements have limitations, including decreased performance during polar nighttime or with high cloud cover (Hall et al., 2004; Holz et al., 2008), which reduces their utility for long-term, consistent monitoring. Passive microwave sensors are increasingly being used, as these are not restricted by time of day or cloud cover (Preußer et al., 2015; Jiang et al., 2020). They can therefore be well suited for generating time series of polynya activity, but their relatively coarse spatial resolution often obscures narrow or irregularly shaped coastal polynyas and can underestimate their true extent. In practice, this can lead to inconsistencies between datasets. For example, the extent and ice production of the largest Arctic coastal polynya, the North Water Polynya, has been estimated differently depending on the resolution of the different sensors used (Tamura and Ohshima, 2011; Iwamoto et al., 2014). With their resolution often being coarse, many coastal polynyas occur at spatial scales that challenge detection by individual sensors alone (Barber and Massom, 2007; Burada et al., 2023). To overcome these limitations, reanalysis products are used to generate high-resolution gridded fields, by assimilating a wide range of data sources, such as multi-sensor satellite observations and in-situ measurements. These integrated datasets can help to address some of the challenges in investigating polynya dynamics consistently across varying spatial and temporal scales. These integrated datasets are particularly powerful for investigating long-term dynamics consistently across space and time, since they combine relatively fine spatial resolution with multi-decadal temporal coverage. This makes them a promising avenue for addressing the current gap in knowledge, as we still lack a clear understanding of how polynyas are changing at long timescales (Mohrmann et al., 2021; Bennett et al., 2024).

1.3 Methods for Polynya Detection

Traditional methods of polynya detection typically rely on sea ice concentration or thickness thresholds, which are used to identify polynyas from sea ice data (Kern et al., 2007; Nakata et al., 2015; Ohshima et al., 2016). Although studies have been conducted to define appropriate detection sea ice concentration and thickness levels, evidence for optimal thresholds which can be used for the identification of both open-ocean and coastal polynyas are still lacking (Massom et al., 1998; Mohrmann et al., 2021). Following the usage of a sea ice threshold, the areal extent of polynyas must then be manually determined to ensure that open ocean and marginal ice zones, which also have sea ice values below the set threshold, are not included within the polynya analysis (Fu et al., 2011). Thresholding approaches also struggle to capture the complex geometry of coastal and irregularly shaped polynyas, which can contain mixed ice-water surfaces and variable concentration gradients that fall between arbitrary cutoff values. As a result, small or fragmented openings are often missed, while large areas of thin or broken ice may

https://doi.org/10.5194/egusphere-2026-1653
Preprint. Discussion started: 26 March 2026

be incorrectly classified as open water. This dependence on fixed thresholds and manual correction introduces subjectivity and inconsistency between studies, particularly when different sensors, resolutions, or regions are compared. These traditional methods are time consuming and as a result have typically been applied to investigate seasonal and interannual polynya dynamics under climate variability (Massom et al., 1998; Tamura and Ohshima, 2011; Campbell et al., 2019). Consequently, they are unsuitable for detecting fine-scale, transient events or for producing automated, reproducible records of polynya variability. The development of an automated and consistent method would enable long-term trends in polynya dynamics under climate change to be explored in a more efficient and accessible way.

Beyond the use of thresholds, a growing number of studies have explored semi- and fully-automated approaches for polynya detection, representing an emerging shift toward objective, reproducible analyses. Early examples include image-processing techniques, such as those using greyscale morphology to estimate sea ice extent (Fu et al., 2012), which removed some subjectivity in boundary definition but remained sensitive to noise and region-specific thresholds. More recently, hybrid methods combining multiple sensors and algorithms have been developed. For instance, Burada et al. (2023) applied supervised and unsupervised classification using Sentinel-1 Synthetic Aperture Radar (SAR) data, which improved coastal polynya delineation but remained constrained by the coarse temporal resolution of SAR and the need for manual validation. Similarly, Heuzé et al. (2021) used spaceborne infrared imagery to identify thermal precursors of Weddell Polynya openings, showing that such data can reveal atmospheric and oceanic preconditioning processes, although their coarse spatial resolution and cloud sensitivity limit broader applicability. The more recent work of Heuzé and Wong (2025) introduced a deep-learning framework capable of automatic Arctic polynya detection, but its reliance on large training datasets and focus on static image classification means performance on long-term, multi-sensor time series remains untested. Collectively, these studies demonstrate the growing promise of automated, data-driven techniques, while highlighting the continuing need for methods that are both transferable and consistent across space, time, and data type.

Automated pattern recognition techniques, utilising algorithms and statistical methods, have long been used in terrestrial environments to classify topographic features into distinct landform types (e.g., Chorowicz et al., 1995; Jasiewicz and Stepinski, 2013). The “geomorphon” algorithm, developed by Jasiewicz and Stepinski (2013), classifies landforms based on local terrain morphology by analysing digital elevation models (DEM) and digital terrain models (DTM). Importantly, parameters within the algorithm can be customised to explore data at a range of spatial resolutions, meaning that the user can produce a landform map relevant to their specific study area and research question(s) (Jasiewicz and Stepinski, 2013; Wyles et al., 2022). Geomorphons have been used for various applications, including landform classification and mapping (Stepinski and Jasiewicz, 2011; Jasiewicz and Stepinski, 2013), predicting soil attributes (Flynn et al., 2020), and detecting treetops in complex forest structures (Antonello et al., 2017). More recently the method has been used with bathymetry data for marine ecological research, investigating the influence of seabed topographic features on the behaviour of shelf sea predators (Wyles et al., 2022). While initially developed for terrestrial geomorphology, the geomorphon algorithm is uniquely adaptable,

https://doi.org/10.5194/egusphere-2026-1653
Preprint. Discussion started: 26 March 2026

meaning that there is potential for its use in cryospheric studies by treating variables such as sea ice concentration as analogous to elevation in topographic models. Since polynyas represent breaks in continuous sea ice cover, they may exhibit distinct geometric patterns when analysed using the geomorphon method. To our knowledge this approach has not yet been used and could provide an automated and consistent method for long-term and fine-scale polynya identification.

1.4 Study Objectives

The overall goal of this study is to explore the utility of the geomorphon pattern recognition algorithm as an automated method for identifying polynyas from sea ice concentration data. This has the potential to improve our ability to investigate polynya dynamics and their trends over long time scales, with important consequences for several processes, such as ecosystem productivity and habitat availability (Gilchrist and Robertson, 2000; Arrigo and van Dijken, 2003; Arrigo et al., 2012; Labrousse et al., 2018), bottom water formation (Comiso and Gordon, 1998; Ohshima et al., 2016), and carbon sequestration (Hoppema and Anderson, 2007; Yager et al., 2016). The specific objectives of this paper are to: (i) Assess the effectiveness of the geomorphon algorithm for polynya detection by applying it to sea ice concentration data and comparing its performance to traditional threshold-based methods, and (ii) evaluate the method's automation potential by running the optimised algorithm on a temporal sea ice concentration dataset and assessing its performance.

2 Data and Methods

2.1 Sea Ice Concentration Data

To evaluate the effectiveness of a method for polynya detection, both coastal and open-ocean polynyas must be considered in the analysis. As a result, two important polynya regions in the Southern Ocean, the Amundsen and Weddell Seas (Morales Maqueda 2004; Macdonald et al., 2023), were chosen for their known presence of coastal and open-ocean polynya systems respectively. Sea ice area fraction data for the two regions was obtained from the Copernicus Global Ocean Physical Multi-Year Product (GLOBAL_MULTIYEAR_PHY_001_030), a reanalysis dataset produced by the Copernicus Marine Environment Monitoring Service (CMEMS) (Lellouche et al., 2021). This variable, henceforth referred to as sea ice concentration, represents the fraction of a grid cell covered by sea ice. The dataset provides global ocean physical variables at a 1/12° horizontal resolution, generated using a data-assimilative ocean model that integrates observational data from satellites and in situ measurements (Lellouche et al., 2021). Sea ice concentration is derived from the NEMO (Nucleus for European Modelling of the Ocean) ocean model (Madec et al., 2024). The dataset offers daily and monthly outputs, making it a well-suited temporal dataset for investigating polynya dynamics.

Sea ice concentration data was downloaded in the format of NetCDF files. Using MATLAB (R2024b), longitude, latitude and sea ice concentration were extracted for the spatial extents of the Amundsen and Weddell Seas (between -130° and -95°

https://doi.org/10.5194/egusphere-2026-1653
Preprint. Discussion started: 26 March 2026

longitude, -80° and -60° latitude, and -90° and 90° longitude, -80° and -50° latitude respectively). This data was then combined with the land-sea mask data extracted from the NetCDF file to generate a sea ice concentration raster (EPSG:4326) in TIFF format for both regions and their respective time periods (Fig. 1). In the final raster, land areas from the land-sea mask were assigned a sea ice concentration value of 1.00, while ocean areas were set to 0.00. For the Weddell Sea, data was selected for October 2017, a month marked by the largest and most persistent occurrence of the Weddell Sea polynya since 1976 (Mchedlishvili et al., 2022; Zhou et al., 2023). Data from December 2020 was used for the Amundsen Sea, when the coastal polynyas here, known for their recurring seasonal presence, were well-documented in previous studies, providing a valuable reference point for comparison (Lee et al., 2022; Macdonald et al., 2023). Monthly mean data was selected to account for the influence of short-term atmospheric and oceanic fluctuations, which can influence polynya formation and persistence on a daily timescale (Macdonald et al., 2023). Therefore, a stable representation of polynya structures is essential for effectively testing the algorithm.

This dataset provides consistent spatial and temporal coverage across both study regions, enabling the geomorphon method to be tested over a long, continuous record. Although previous studies have often relied on short time series or region-specific datasets, our approach uses data with sufficient resolution in both space and time to evaluate detection performance comprehensively and reproducibly.

https://doi.org/10.5194/egusphere-2026-1653
Preprint. Discussion started: 26 March 2026

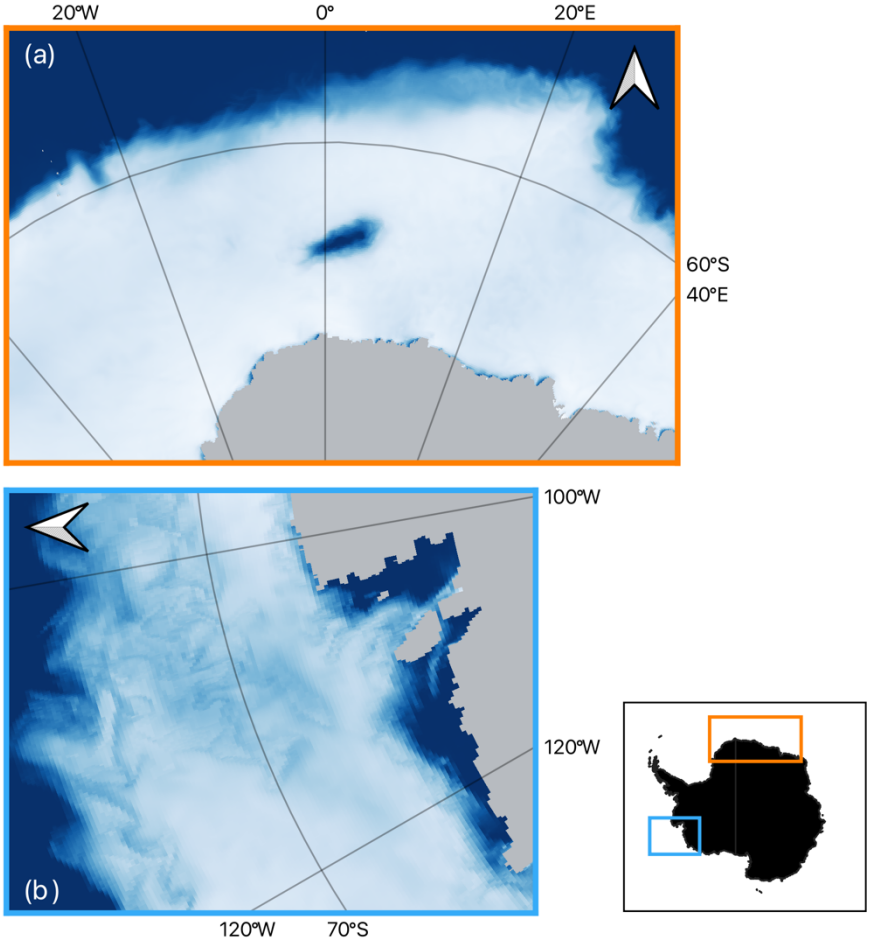

Figure 1: Monthly sea ice concentration for the (a) Weddell Sea in October 2017, and (b) Amundsen Sea in December 2020. Insert shows the location of the Weddell Sea (orange) and Amundsen Sea (blue) on a larger scale. Monthly mean data was obtained from the Copernicus Global Ocean Physical Multi-Year Product (Lellouche et al. 2021).

2.2 Defining Polynyas for Detection

Due to the variation in definitions of polynyas discussed in the introduction, we adopt here a morphological definition of a polynya: a distinct open-water depression within the surrounding sea ice cover, characterised by low or no sea ice, that is entirely isolated from the open ocean. This definition captures both coastal polynyas, where open water is bounded by continuous sea ice on one side and the coastline on the other, and open-ocean polynyas that are fully enclosed by continuous sea ice. No persistence or temporal duration criteria are applied, as the aim of this study is to evaluate the method's ability to detect polynyas rather than to analyse their temporal evolution. This morphological definition aligns directly with the geomorphon approach, which objectively identifies depressions based on spatial form rather than fixed sea ice concentration

https://doi.org/10.5194/egusphere-2026-1653
Preprint. Discussion started: 26 March 2026

thresholds. At the same time, it remains compatible with traditional sea ice concentration threshold-based methods, as it identifies regions of reduced sea ice concentration that would typically fall below conventional cutoff values. As such, it provides a consistent framework for comparing the geomorphon-derived results with those obtained using sea ice concentration based detection techniques.

2.3 Geomorphon Algorithm for Polynya Detection

Using DTM input data with a known spatial resolution (e.g., 250 m), the geomorphon pattern recognition algorithm produces a raster layer in which each grid cell is assigned one of the 10 most commonly recognisable landform elements associated with a terrestrial landscape (Fig. 2) (Jasiewicz and Stepinski, 2013). The algorithm requires the user to define three parameters which influence the classification of geomorphological features (Stepinski and Jasiewicz, 2011). The first is the search radius (*search*), which represents the maximum distance (m) from the central cell that the algorithm searches out from. The *search* parameter represents the number of map cells, and as a result, a DTM with a 300 m resolution and *search* equal to 10, corresponds to a search radius of 3,000 m. Notably, the algorithm automatically determines the optimal lookup distance for each cell in a self-adaptive manner. As a result, this parameter should have a relatively large value which encompasses the maximum extent of a landform, as this enables the algorithm to identify landform elements on a wider range of spatial scales (e.g., narrow and wide valleys) (Stepinski and Jasiewicz, 2011). If the value of *search* is too small, landforms larger than *search* will be broken down into individual landform components. The second parameter, flatness threshold (*flat*), is the slope gradient (degrees) that is considered flat. Any gradient above this threshold is considered a deviation from a flat geomorphon and thus will represent one of the other 9 common landform elements. The third parameter is the spatial resolution of the DTM data, the value of which depends on what data source you are utilising. An additional optional parameter, flat distance (*dist*), can also be incorporated which defines the distance, measured in map cells, beyond which the algorithm gradually reduces the *flat* threshold. This prevents surfaces with a gradual slope from being misclassified as flat by accounting for elevation change which might occur over large distances. This is an important parameter to adjust when the spatial resolution of the user's DTM is low. The ability to adjust these parameters allows for the creation of a landform map that is specific to the user's spatial resolution and research question(s) of interest.

https://doi.org/10.5194/egusphere-2026-1653
Preprint. Discussion started: 26 March 2026

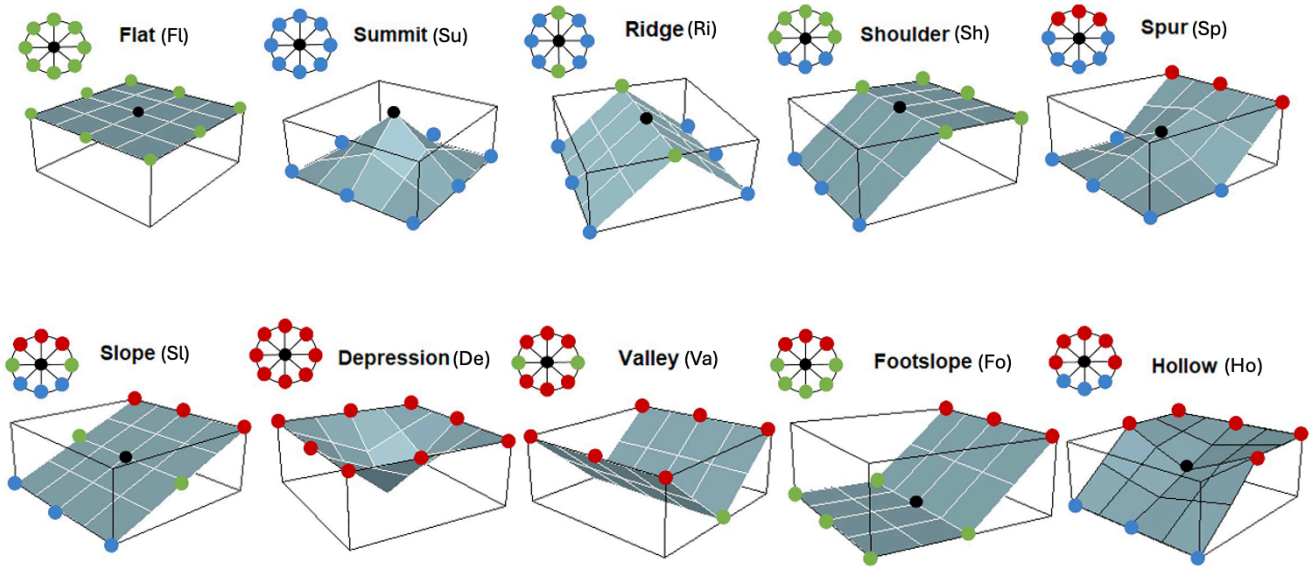

Figure 2: Symbolic 3D morphologies and their coordinating geomorphons (ternary patterns) for the 10 most common landform elements (adapted from Jasiewicz and Stepinski, 2013 and Wyles et al., 2022). Coloured points demonstrate if the cells surrounding the central cell (black) are lower (blue), higher (red), or the same elevation (green) as the central cell.

255

The geomorphon method utilises a line-of-sight principle for investigating the relationship of a central cell with its neighbouring cells in the DTM raster (Yokoyama et al., 2002). This means that the lookup distance is incrementally extended up to the predefined maximum value to determine the minimum zenith and nadir angles along eight compass directions from the central grid cell (Stepinski and Jasiewicz, 2011). These angles are then assessed to establish whether neighbouring cells 260 are higher, lower, or the same elevation as the central cell. This classification is encoded into a ternary pattern which represents the geomorphon. Theoretically, there are 6,561 possible topographic patterns, however, to reduce this for mapping they are condensed into the 10 most common landforms: flat, summit, ridge, shoulder, spur, slope, depression, valley, footslope, hollow (Fig. 2) (Jasiewicz and Stepinski, 2013). As a result, the output of the algorithm is a raster with values for each grid cell equivalent to one of these 10 landforms. Similar to changes in elevation seen in a DTM, variations in sea ice concentration 265 across a body of water can produce unique spatial structures (Fig. 3). By applying the geomorphon algorithm to this data, it may be possible to determine polynyas from sea ice concentration structures that resemble certain classic landforms, such as valleys, depressions and hollows.

https://doi.org/10.5194/egusphere-2026-1653
Preprint. Discussion started: 26 March 2026

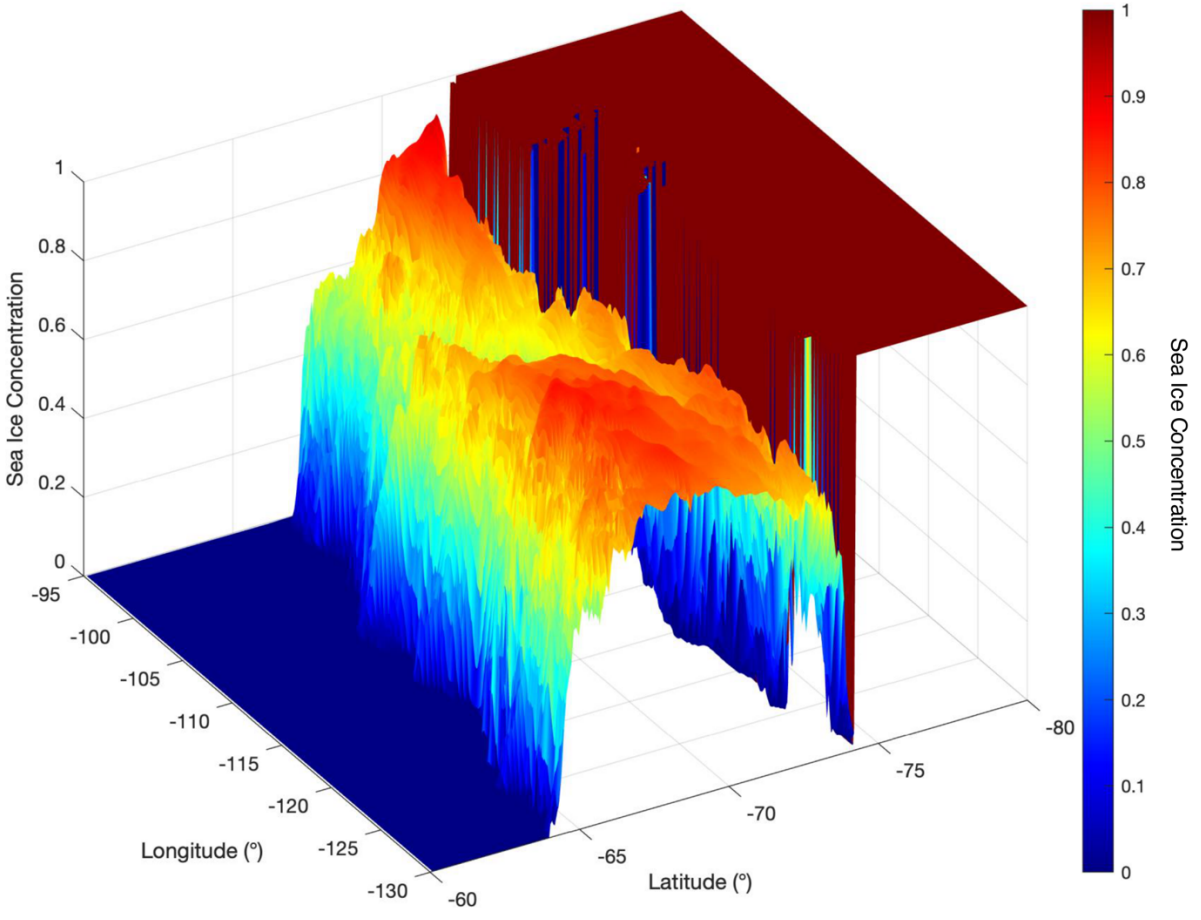

Figure 3: The 3D structure of sea ice concentration in the Amundsen Sea, December 2020. The dark blue steep declines in sea ice concentration seen near the coastline represents areas of coastal polynyas as seen in Fig. 1. Monthly mean data was obtained from the Copernicus Global Ocean Physical Multi-Year Product (Lellouche et al. 2021).

To ensure compatibility with the geomorphon algorithm, which requires all distance parameters (*search* and *dist*) to be expressed in meters, sea ice concentration data was first reprojected from geographic coordinates (EPSG:4326, latitude/longitude) to a polar stereographic projection (EPSG:3031), which uses meters as its units. To maintain consistency and ensure the geomorphon algorithm's distance-based parameters were comparable across both the Amundsen and Weddell Seas, a uniform target resolution of 9,250 m was selected during reprojection. This resolution was chosen to align with the original horizontal resolution of the Copernicus dataset, as 1° of latitude at the equator corresponds to approximately 111 km, making the original data's 1/12° resolution equivalent to 9,250 m.

https://doi.org/10.5194/egusphere-2026-1653
Preprint. Discussion started: 26 March 2026

In order to determine the most suitable parameters for identifying polynyas from sea ice concentration data, a range of values for *search*, *flat*, and *dist* parameters were trialled with sea ice concentration data of a set spatial resolution (9,250 m). The *search* parameter is measured in map cells and as a result requires knowledge of the spatial resolution of the sea ice concentration data and the size of the landform you are trying to classify to determine its value. A broad range of *search* values were tested, relating to varying search distances and resultant maximum landform sizes (Table 1). Smaller values were used for the Amundsen Sea, as coastal polynyas typically reach a smaller size than those which are open-ocean (Mohrmann et al., 2021).

To adapt the geomorphon algorithm for sea ice concentration data, the *flat* parameter was reinterpreted in terms of sea ice concentration gradients. The spatial resolution of the data (9,250 m) was used to convert differences in sea ice concentration between adjacent grid cells into slope angles. Specifically, the *flat* angle threshold (in degrees) was calculated using the inverse tangent function following Eq. (1):

$$\theta = tan^{-1}\left(\frac{\Delta SIC}{d}\right), \quad (1)$$

where ΔSIC is the difference in sea ice concentration between the central cell and its neighbours, and d is the horizontal distance between grid cells (9,250 m). For example, a sea ice concentration difference of 0.4 corresponds to a slope angle of approximately 0.0025°, which is then used as the *flat* threshold value to classify any changes above this as “not flat”. A spectrum of *flat* parameter values were chosen to encompass a range of sea ice concentration thresholds which might be used for landform classification (Table 2). The same six values were used for both the Weddell and Amundsen Seas. Finally, four values of the *dist* parameter were used (1, 2, 3, and 4) for both the Weddell and Amundsen Seas.

Having defined the parameter combinations and spatial resolution of the sea ice concentration data, the Geographic Resources Analysis Support System (GRASS GIS) (Neteler and Mitasova, 2007) extension r.geomorphon (Jasiewicz and Stepinski, 2013) was used to calculate geomorphons in R. As a result, the geomorphon algorithm was run with a total of 96 (4*6*4) parameter combinations for the Weddell Sea and 144 (6*6*4) for the Amundsen Sea.

https://doi.org/10.5194/egusphere-2026-1653
Preprint. Discussion started: 26 March 2026

Table 1: *Search* parameter values used to test geomorphon algorithm on sea ice concentration data for the Amundsen and Weddell Seas. Each search distance corresponds to a maximum landform size (km²).

Search parameter (map cells)	Landform size (km²)	Weddell Sea	Amundsen Sea
2	~1100	×	✓
5	~6700	×	✓
10	~27000	×	✓
15	~65000	✓	✓
20	~110000	✓	✓
30	~240000	✓	✓
40	~430000	✓	×

Table 2: *Flat* parameter values, and their corresponding sea ice concentration thresholds, used to test geomorphon algorithm on sea ice concentration data for the Amundsen and Weddell Seas.

Flat parameter	Corresponding sea ice concentration threshold
0.00015	0.025
0.00031	0.05
0.00062	0.1
0.0012	0.2
0.0025	0.4
0.005	0.8

2.4 Threshold-Based Method for Polynya Detection

Sea ice concentration thresholds are the most widely used and well established method for the detection of polynyas. As such, it is used in our study as the benchmark against which to evaluate the performance of the geomorphon detection approach. This allows for direct comparison between a well-established, threshold-based classification and the novel morphological method presented in this study.

To determine polynya areas using the traditional threshold-based method, the sea ice concentration raster for both regions was imported into QGIS (version 3.42), and two grids were created, one for the Amundsen Sea and one for the Weddell Sea. These grids were set to have the same spatial resolution as the sea ice concentration data (1/12° EPSG:4326). The geoprocessing toolbox was then used to sample values from the Amundsen and Weddell Seas sea ice concentration rasters onto their

https://doi.org/10.5194/egusphere-2026-1653
Preprint. Discussion started: 26 March 2026

respective gridded fields. A new polynya detection threshold variable was created using the field calculator, where grid points with sea ice concentration lower than 0.3 were assigned the value 1, and those with higher sea ice concentrations were assigned 0. The value of 0.3 was chosen as a study reviewing detection thresholds found that this provided a suitable balance between detecting polynyas effectively and avoiding incorrect classifications (Morhmann et al., 2021). Higher thresholds risk underestimating polynyas by excluding those which may have regional areas of sparse sea ice cover, while lower thresholds tend to misclassify embayments as polynyas (Morhmann et al., 2021).

Using this detection threshold, polygons were manually drawn around grid points classified as polynyas by creating a new shapefile and adding polygon features for each region. Polygons were drawn using a dot-to-dot method to connect adjacent qualifying points, ensuring a systematic and repeatable identification process. Polygons were not drawn around ice-free areas beyond the sea ice extent, as these represented open ocean. The geoprocessing toolbox was then used to define a polynya variable, assigning a value of 1 to grid points within polygons, and 0 to those outside.

2.5 Statistical and Spatial Analysis

To test the effectiveness of using the geomorphon algorithm for polynya identification, detected valley, depression and hollow landforms from each algorithm iteration were compared to polynya areas defined using the traditional method of a set sea ice concentration threshold. The landforms valley, depression and hollow were chosen as these represent morphologies where the majority of neighbouring cells to the central cell are higher in elevation, thus closely mimicking a polynya, an area of low sea ice concentration surrounded by high sea ice concentration.

To enable comparative analysis, the sea ice concentration raster containing the polynya areas defined by the threshold-based method was combined with the geomorphon-derived landform classifications. Using the ‘Sample raster values’ tool in QGIS, values were sampled from all 96 and 144 iterations of the geomorphon algorithm for the Weddell and Amundsen Seas respectively. This resulted in a final gridded field containing longitude, latitude, sea ice concentration, threshold-based polynya classification, algorithm parameter combinations, and landform classifications for each region. The final gridded field was exported as a CSV file, which was analysed in R.

Performance of the geomorphon algorithm was quantified using precision, recall, and F-1 scores which are commonly used evaluation metrics for classification tasks (e.g., Behera et al., 2019; Alem and Kumar, 2022). Precision measures the proportion of correctly identified polynyas among all detected polynyas, providing insight into how many of the identified features are actually true positives (Cook and Ramadas, 2020). Recall, on the other hand, assesses the proportion of polynyas identified by the threshold-based method that were correctly detected by the algorithm, indicating how well it captures actual polynya areas (Cook and Ramadas, 2020). The F1-score, which is the harmonic mean of precision and recall, balances these two metrics, ensuring that both false positives and false negatives are taken into account (Albaji et al., 2023). This combination of metrics

https://doi.org/10.5194/egusphere-2026-1653
Preprint. Discussion started: 26 March 2026

allows for a comprehensive assessment of the algorithm's ability to accurately identify polynyas while minimising misclassification errors. To further validate the algorithm's effectiveness, visual and spatial comparisons were conducted for the best-performing parameter iterations, examining how well the detected landforms aligned with known polynya areas.

The best-performing parameter combination across both regions was determined by ranking the parameter combinations separately for each region based on their F1-score. Each combination was assigned a rank within its respective region (1 = highest F1-score). We then apply a rank aggregation approach, summing the rankings from both regions to identify the best overall performer. This parameter combination was used to re-run the geomorphon algorithm on a 12-month time series of sea ice concentration data, with the Weddell Sea analysed for 2017 and the Amundsen Sea for 2020. The total polynya area for each month was measured and compared with results from polynya area detected by the sea ice concentration threshold-based method.

2.6 Transferability Across Sea Ice Concentration Datasets

To assess the transferability of the geomorphon detection method across sea ice concentration products with differing spatial resolution and retrieval methodologies, the best-performing parameter combination derived from the Copernicus reanalysis dataset was analytically rescaled and applied to an independent passive microwave sea ice concentration product. This dataset was the University of Bremen Arctic and Antarctic Sea Ice (ASI, version 5.4) product, which applies the ARTIST Sea Ice algorithm to Advanced Microwave Scanning Radiometer 2 (AMSR2) brightness temperature observations from the JAXA GCOM-W1 satellite to produce daily Antarctic sea ice concentration fields at 6.25 km resolution (Melsheimer and Spreen, 2019). This dataset differs from the Copernicus product in both spatial resolution and data retrieval approach, providing an opportunity to evaluate whether the geomorphon method can be consistently applied across independent observational sources. Parameter rescaling preserved the physical interpretation of each geomorphon parameter rather than relying on empirical re-optimisation. The flat threshold was recalculated using Eq. (1), ensuring equivalence with the same sea ice concentration gradient between neighbouring grid cells. The search parameter was adjusted to maintain a corresponding maximum detectable landform area, thereby preserving the upper spatial scale of identifiable polynyas. Similarly, the dist parameter was scaled to maintain a comparable lookup distance relative to the dataset resolution, preventing gradual concentration gradients from being misclassified as flat surfaces. The method was applied to the Amundsen Sea region.

3 Results

To assess the performance of the geomorphon algorithm in identifying polynyas, we evaluated a range of parameter combinations across the Weddell and Amundsen Seas, and compared the classification results to those obtained using the 0.3 sea ice concentration threshold-based method. Across all tested parameter combinations, we examined the most frequently

https://doi.org/10.5194/egusphere-2026-1653
Preprint. Discussion started: 26 March 2026

assigned geomorphon landforms at areas classified as polynyas and non-polynyas by the threshold-based method (Fig. A1). The three most common geomorphon landforms associated with polynyas were the same across both the Amundsen and Weddell Sea, being flat (41.2%, 33.6%), footslope (27.3%, 21.2%), and hollow (15.1%, 16.2%). For the Weddell Sea, depression (13.4%) and slope (11.8%) landforms were also commonly associated with polynyas. Depressions (2.3%) and slopes (2.6%) were associated much less in the Amundsen Sea, with valleys being more commonly associated (10.4%). For non-polynya regions (i.e., areas of open ocean or sea ice concentration > 0.3), flat landforms were the most common for both the Amundsen (86.8%) and Weddell (76.9%) Seas. In the Weddell Sea, shoulder (8.4%) and slope (8.6%) were also commonly associated with non-polynya areas. The same pattern occurs in the Amundsen Sea, but with smaller proportions of shoulder (4.7%) and slope (2.1%) landforms classified in non-polynya areas.

There was considerable variability in precision and recall scores across parameter combinations (Fig. B1). Across all parameter combinations, the algorithm achieved higher average precision in the Weddell Sea (0.44) than in the Amundsen Sea (0.42), whereas average recall was greater in the Amundsen Sea (0.45) compared to the Weddell Sea (0.41). The broader spread in precision-recall scores observed for the Amundsen Sea reflects the greater variation in search radius values used during algorithm iterations. Examining precision and recall by specific parameter values reveals that higher *search* values (> 15 map cells) yield higher precision and recall scores in both the Amundsen and Weddell regions (Fig. B2). Algorithm iterations for both regions with increasing values of *flat* thresholds were observed to have higher precision scores, but lower recall. Varying values of the *dist* parameter used in the algorithm had less of an effect on precision and recall scores for both regions.

Given the variability in precision and recall, F1-scores also exhibited considerable variation across both regions, with certain parameter combinations yielding notably higher classification success than others (Fig. 4 and 5). For the Weddell Sea October 2017, the highest F1-scores (> 0.8) were achieved by iterations of the algorithm which included *flat* thresholds of 0.00062°, 0.0012°, or 0.0025° (Fig. 4). The lower *flat* thresholds achieved a higher F1-score when combined with a higher *dist* parameter value, whilst the higher *flat* values attained higher F1-scores when paired with lower *dist* values. The highest F1-scores were also seen when the *search* distance parameter had values of 20, 30, and 40 map cells. The best performing combination of parameter values achieved an F1-score of 0.85 and included a *flat* threshold of 0.0012°, *search* distance of 20 map cells, and *dist* parameter of 2. The same general pattern is observed for the Amundsen Sea December 2020, whereby *flat* thresholds of 0.00062°, 0.0012°, or 0.0025° achieved the highest F1-scores (> 0.8), with the lower *dist* parameter values attaining higher F1-scores when paired with higher *flat* thresholds and vice versa (Fig. 5). Higher values of the *search* parameter also yielded the highest F1-scores, with 15, 20, and 30 map cells performing the best. For the Amundsen Sea, the best performing parameter combination achieved an F1-score of 0.89 with a *flat* threshold of 0.0025°, *search* distance of 20 map cells, and *dist* parameter of 1.

https://doi.org/10.5194/egusphere-2026-1653
Preprint. Discussion started: 26 March 2026

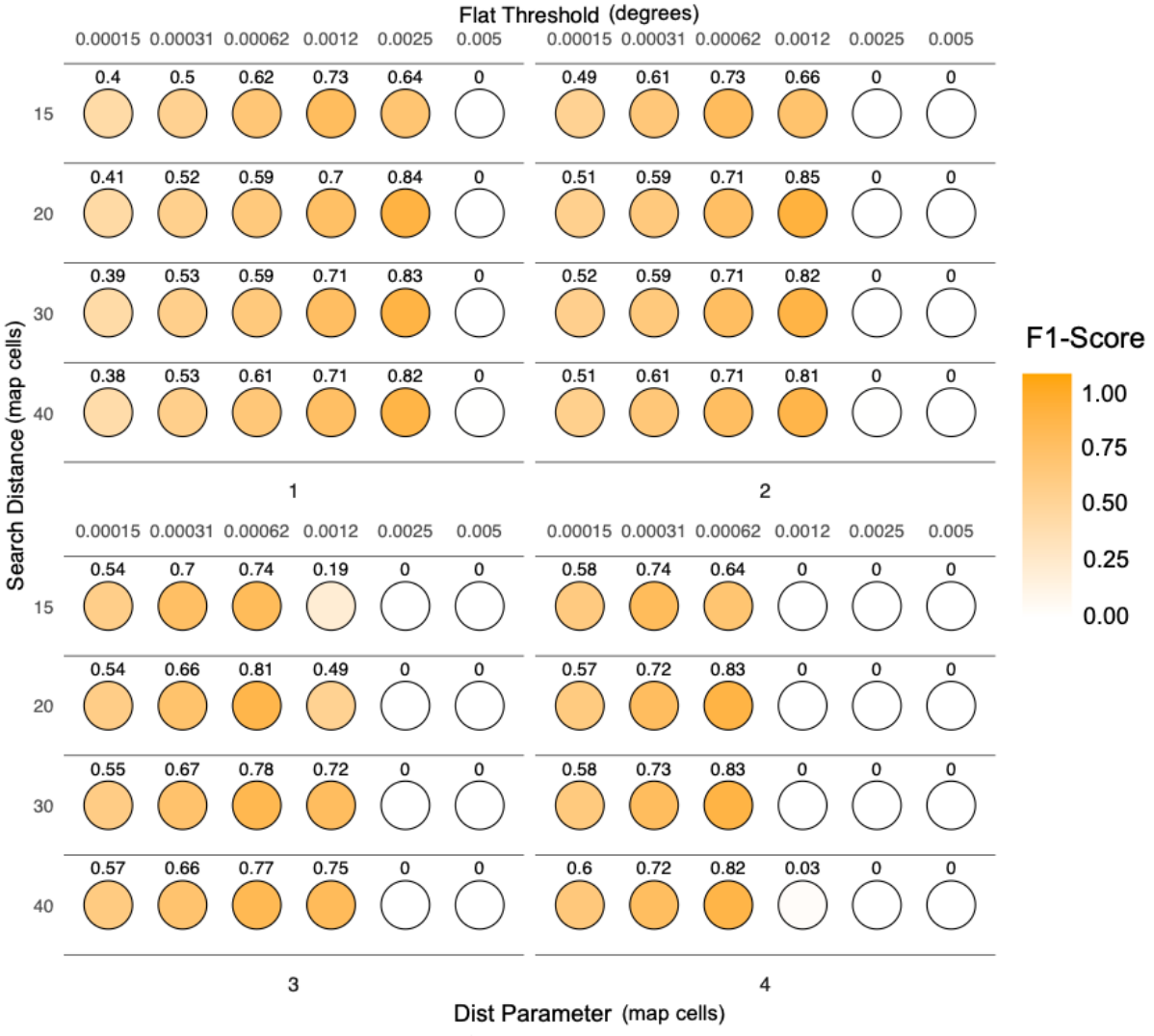

Figure 4: F1-scores for all tested parameter combinations of the geomorphon algorithm for the Weddell Sea. Each dot represents a unique combination of *search*, *flat*, and *dist* parameters, with shading corresponding to F1-score. Higher F1-scores indicate better agreement between geomorphon classifications and polynya areas defined by the 0.3 sea ice concentration threshold-based method.

https://doi.org/10.5194/egusphere-2026-1653
Preprint. Discussion started: 26 March 2026

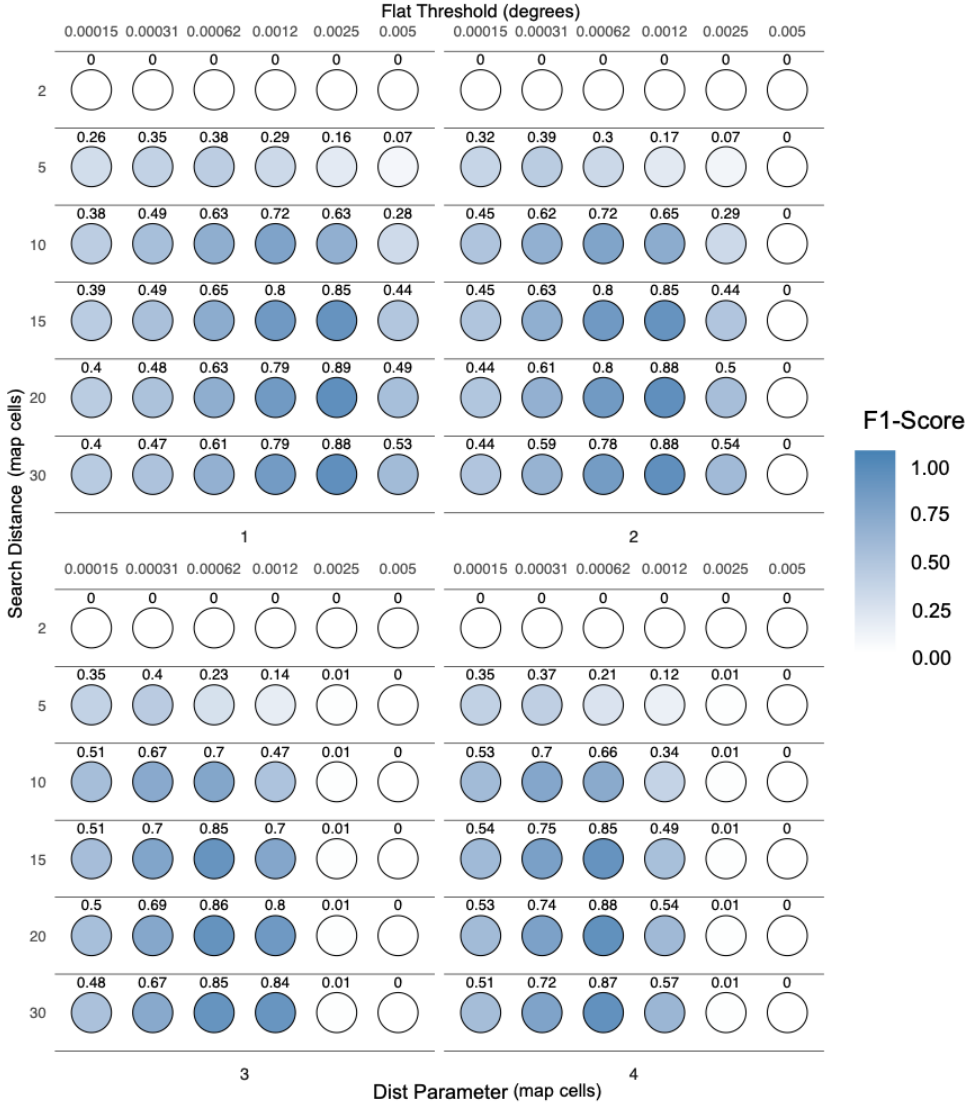

Figure 5: F1-scores for all tested parameter combinations of the geomorphon algorithm for the Amundsen Sea. Each dot represents a unique combination of *search*, *flat*, and *dist* parameters, with shading corresponding to F1-score. Higher F1-scores indicate better agreement between geomorphon classifications and polynya areas defined by the 0.3 sea ice concentration threshold-based method.

The parameter combination with a *flat* threshold of 0.0025°, *search* radius of 20 map cells, and *dist* parameter of 1, achieved the lowest combined rank, ranking 1 in the Amundsen Sea and 2 in the Weddell Sea, making it the best-performing combination overall. When compared visually with the polynyas identified using the sea ice concentration threshold (< 0.3) method, the geomorphon-detected polynya identifying landforms produced by this parameter set, show strong spatial agreement, as valleys, depressions and hollows align closely with polynya areas defined by the threshold-based method (Fig. 6).

https://doi.org/10.5194/egusphere-2026-1653
Preprint. Discussion started: 26 March 2026

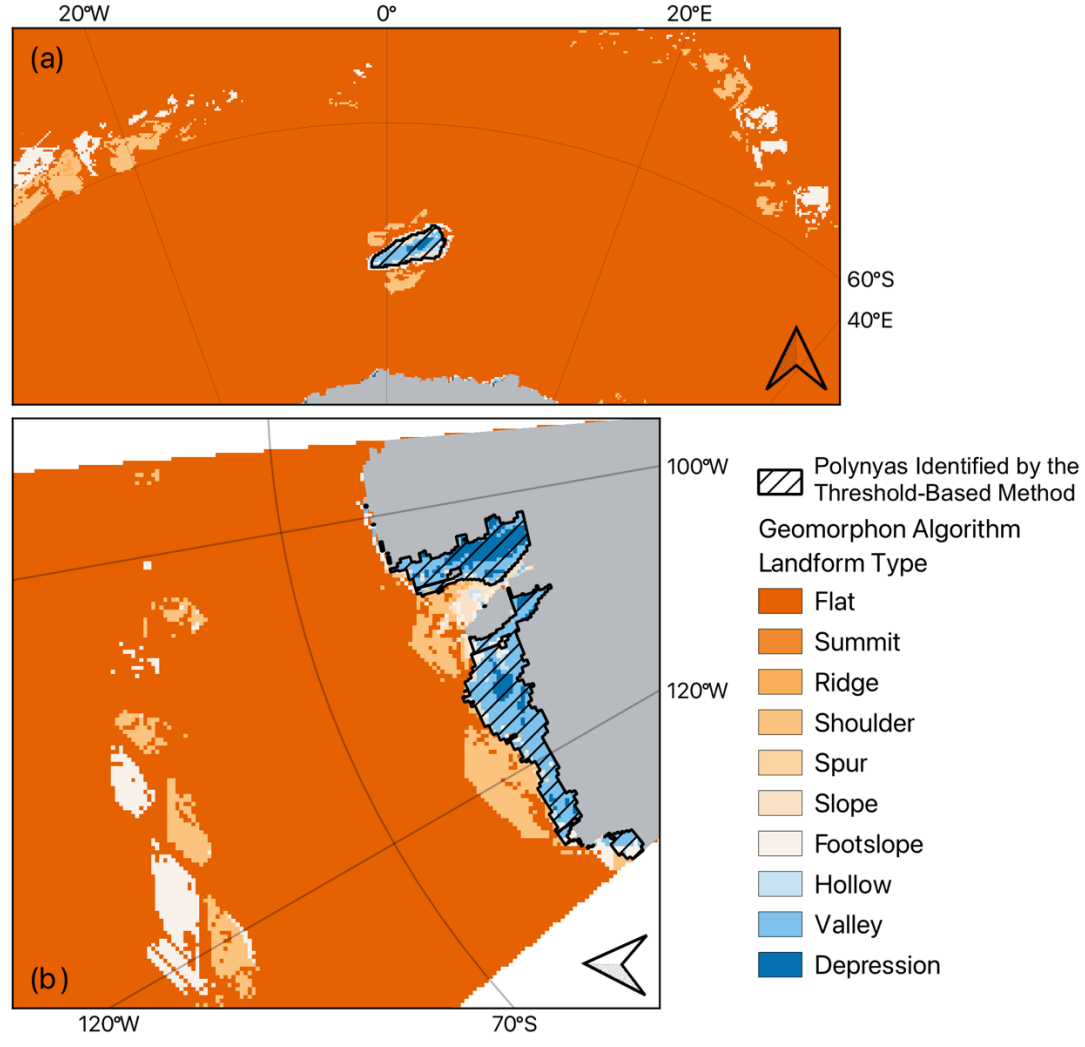

Figure 6: Geomorphon landform classifications using the best performing parameter combination (*flat* = 0.0025°, *search* = 20 map cells, *dist* = 1 map cells) in the (a) Weddell Sea and (b) Amundsen Sea. Areas identified as polynyas using the sea ice concentration threshold (< 0.3) are outlined in black hatching. Geomorphon-detected landforms associated with polynya presence are those in shades of blue, whilst those identifying non-polynya areas are in shades of orange.

Panels (a) and (b) of Figure 7 show the monthly variation in polynya area in the Weddell and Amundsen Seas for 2017 and 2020 respectively. Both methods display broadly similar seasonal trends in polynya area, with the largest polynya area observed in austral spring-summer months (September-February), and smallest in austral winter. In the Weddell Sea the geomorphon algorithm appears to underestimate polynya area when compared to the sea ice concentration threshold-based method. Generally, the opposite is observed in the Amundsen Sea where the geomorphon algorithm predicts slightly higher polynya area in the majority of months. Panel (c) demonstrates the scalability of the geomorphon method, presenting daily

https://doi.org/10.5194/egusphere-2026-1653
Preprint. Discussion started: 26 March 2026

resolution results for the Amundsen Sea in 2020. The method captures short-term fluctuations in polynya area, including periods of rapid growth and decline, such as those observed in austral spring and summer months.

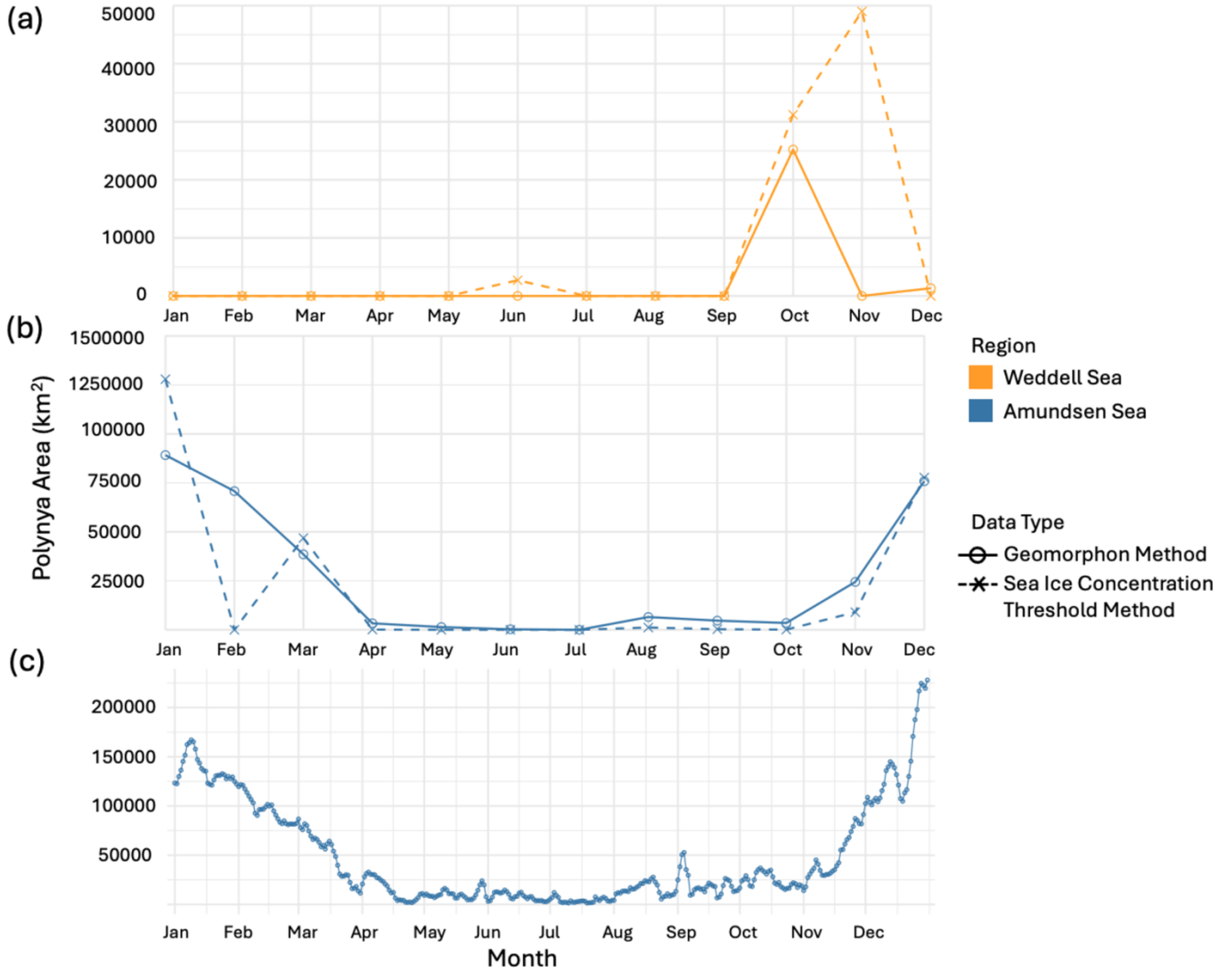

Figure 7: Comparison in monthly polynya area (km²) in the (a) Weddell Sea 2017 (orange) and (b) Amundsen Sea 2020 (blue), determined by the geomorphon algorithm, using the best performing parameter combination (*flat* = 0.0025°, *search* = 20, *dist* = 1), and the sea ice concentration threshold (< 0.3) method. Daily polynya area using the geomorphon algorithm was also determined for the Amundsen Sea 2020 (panel c).

To further evaluate the transferability of the geomorphon method, the analytically rescaled parameter configuration was applied to the independent AMSR2 University of Bremen sea ice concentration dataset. Parameter scaling resulted in a *flat*

https://doi.org/10.5194/egusphere-2026-1653
Preprint. Discussion started: 26 March 2026

threshold of 0.0036° (corresponding to a sea ice concentration threshold of 0.4), a *search* distance of 30 map cells (equivalent to a maximum landform size of ~110,000 km^2) , and a *dist* parameter of 1.5 map cells (equal to ~9 km), preserving equivalence with the physical interpretation of the optimised Copernicus parameter set despite differences in grid resolution. Application of the method produced consistent identification of coastal polynyas within the Amundsen Sea, with detected spatial area closely matching that obtained using the Copernicus dataset (Fig. C1). Minor differences between datasets, most notably during late summer conditions, primarily reflect contrasts in sea ice concentration gradients associated with differing retrieval methodologies and spatial resolution of the datasets, with the assimilated Copernicus product generally producing larger detected polynya areas relative to the passive microwave AMSR2 observations. Polynya boundaries and areal extents remained well resolved despite the change in data type and spatial resolution, indicating that geomorphon-derived landform classifications respond primarily to relative spatial gradients in sea ice concentration rather than dataset-specific characteristics.

4 Discussion

This study aimed to evaluate the potential of the geomorphon pattern recognition algorithm as an automated tool for detecting polynyas within sea ice concentration data. By systematically testing multiple parameter combinations across two distinct and significant polynya regions, our results demonstrate that the algorithm can effectively identify polynyas. Applying the best parameter combination to time series data enables investigations into changes in occurrence and size over time. This approach offers a novel, time efficient means, of capturing spatial and temporal dynamics in polynya formation and persistence, providing valuable insights into their variability, which can support improved monitoring and understanding of these oceanographic features. As interest grows in developing automated approaches for mapping polar ocean features, this study contributes a timely advancement by demonstrating a technique that is both computationally efficient and conceptually aligned with the morphological nature of polynyas.

4.1 Evaluating Landform Classification in Polynya Detection

Specific geomorphon landforms showed clear associations with polynya and non-polynya areas, providing evidence that distinct surface morphology patterns correspond to the presence or absence of open water features within sea ice fields. Landforms such as hollows, footslopes, and depressions were commonly represented in polynya regions, suggesting these terrain types effectively capture localised reductions in sea ice concentration. Conversely, flat landforms were more common in non-polynya areas, likely reflecting regions of persistently high or low sea ice cover, either consolidated ice or permanent open water, with minimal structural complexity. Shoulders, ridges, and spurs also occurred more frequently outside polynya regions, potentially representing the structured and consolidated ice typical of surrounding pack ice (Comiso et al., 2003; Andersen et al., 2007). These spatial associations align with physical expectations and support the utility of the geomorphon method in capturing morphologies relevant to sea ice concentration patterns.

https://doi.org/10.5194/egusphere-2026-1653
Preprint. Discussion started: 26 March 2026

Some overlap between geomorphon landform categories across polynya and non-polynya regions highlights the importance of spatial context and careful parameter tuning in improving classification accuracy. For instance, footslope landforms were frequently associated with polynya regions across the full set of parameter combinations tested, however, in the best-performing configurations, these features were primarily concentrated along the boundary between the marginal ice zone and the open ocean (Fig. 6). This spatial distribution is consistent with the geomorphon definition of footslopes, as transitional features between lower and higher elevations (Fig. 2), analogous to the sea ice concentration gradients found at the ice edge where open water transitions to consolidated pack ice (Worby and Comiso, 2004; Bitz et al., 2005). Identifying valleys, depressions, and hollows as the core landforms for polynya detection is therefore a critical step in tailoring the geomorphon algorithm for this application. These features most closely represent the morphological patterns associated with low sea ice concentration in polynyas. In contrast, landforms such as flats, footslopes, and slopes, appear in polynya areas under many parameter combinations, but also correspond to other sea ice or open ocean structures not characteristic of polynyas. Including them as primary indicators would risk misclassification and reduce the specificity of the method. As such, deliberate selection and tuning of relevant landform features is essential to ensure robust and accurate polynya identification.

4.2 Parameter Sensitivity and Algorithm Performance

Performance metrics revealed substantial variation across the 144 and 96 parameter combinations tested for the Amundsen and Weddell Seas respectively, highlighting the importance of tuning the algorithm to the scale and context of polynya identification. Overall, the best-performing iterations of the algorithm included a moderate *search* distance of 20 map cells, and slightly higher *flat* threshold of 0.0025°, combined with the lowest *dist* parameter value (Fig. 6). In the context of the Copernicus sea ice concentration data, these parameter values translate to a search radius of 185 km, which equates to a maximum polynya area of ~110,000 km^2, and a sea ice concentration threshold of 0.4 (Table 1 and 2). These values are consistent with the known oceanographic characteristics of polynyas, as they typically range in size from 10 to 10^5 km^2 (Barber et al., 2001). This aligns closely with the search radius identified as optimal in our analysis, supporting the suitability of the chosen *search* parameter. Moreover, sea ice concentration within polynyas varies considerably, especially in coastal polynyas which are sites of vast sea ice production (Tamura and Ohshima, 2011; Zhou et al., 2023). As a result, the best-performing *flat* threshold corresponding to a moderate sea ice concentration threshold is understandable, as polynyas are not always homogenous areas of open water surrounded by high sea ice concentration (Kwok et al., 2007; Gutjahr et al., 2016).

The areal extents of polynyas identified for the two regions using the geomorphon algorithm align closely with those reported in scientific literature, reinforcing the validity of this method for capturing realistic spatial patterns of polynyas. Antarctic coastal polynyas, like those observed in the Amundsen Sea, typically range in size between 130-20,000 km^2 (Barber and Massom, 2007). The largest total polynya area detected in this region by the geomorphon algorithm was 127,931 km^2 in January 2020, with individual polynya size ranging from 16 km^2 to 29,421 km^2 (Fig. 7). These figures are consistent with expectations for the Amundsen Sea region, where the literature reports that the largest feature, the Amundsen Sea Polynya,

https://doi.org/10.5194/egusphere-2026-1653
Preprint. Discussion started: 26 March 2026

can reach between 25,000 and 40,000 km² during the austral summer (van Manen et al., 2022; Macdonald et al., 2023). In austral winter, polynya size of the Amundsen Sea Polynya was estimated at 7,700 +/- 3,600 km² between 2003 and 2011 (Macdonald et al., 2023). Unlike the sea ice concentration threshold-based method, the geomorphon algorithm is capable of detecting polynyas in the Amundsen Sea during the austral winter. However, the total polynya area observed is lower than literature suggests. For the Weddell Sea polynya, the Moderate Resolution Imaging Spectroradiometer on NASA's Terra satellite acquired images of the polynya in 2017 in the eastern Weddell Sea, observing it grow from 9,500 km² in mid-September, to approximately 80,000 km² by late October (Jena et al., 2019). The geomorphon algorithm identified the polynya in the same area and detected the large increase in size from September to October (Fig. 7). However, the algorithm appears to fail to detect its presence in the austral winter months when compared to the sea ice concentration threshold-based method. These discrepancies observed in both regions may stem from the use of monthly-averaged sea ice concentration data, which can smooth over transient or short-lived open water events (Macdonald et al., 2023). As shown in this study (Fig. 7c), applying the geomorphon method to daily sea ice concentration data in the Amundsen Sea markedly improves the detection of short-lived and small-scale polynya openings. The daily time series captures brief expansions and closures that are obscured in monthly averages, demonstrating the method's sensitivity to rapid changes in sea-ice conditions. This preliminary application highlights the potential of the geomorphon approach for long-term, high-temporal-resolution monitoring of polynya dynamics over several decades.

A major advantage of the geomorphon algorithm lies in its ability to dynamically determine the optimal lookup distance for each cell, allowing it to identify landforms across a spectrum of spatial scales (Stepinski and Jasiewicz, 2011). This flexibility is particularly valuable for detecting polynyas, where size can vary significantly, even within a single region, due to short-term meteorological influences such as wind and air temperature (Stringer and Groves, 1991; Wang et al., 2021). In the Amundsen Sea, for instance, the algorithm successfully captured coastal polynyas of varying sizes, with the largest and smallest polynyas observed covering areal extents of 46,855 km² and 12 km² respectively (Fig. 6), illustrating the algorithm's ability to detect polynyas at a wide range of spatial scales.

4.3 Comparison with Threshold-Based Method

One of the key advantages of the geomorphon algorithm lies in its high degree of automation, which marks a significant step forward from more labour-intensive methods such as manual delineation or static sea ice concentration threshold-based approaches. While this study used monthly-averaged sea ice concentration data to test the algorithm's effectiveness, this temporal resolution likely smooths over many short-lived or transient polynya events, particularly in winter, when these features are more variable due to short-term meteorological influences (Stringer and Groves, 1991; Wang et al., 2021). The strength of the geomorphon method, however, is that it can be easily scaled to higher temporal resolutions without significantly increasing processing demands. Notably, this approach can process a 12-month time series of monthly averaged sea ice concentration data in minutes, reducing computational time by roughly two orders of magnitude, relative to the conventional

https://doi.org/10.5194/egusphere-2026-1653
Preprint. Discussion started: 26 March 2026

570 threshold-based method used for comparison. Because the algorithm is automated and extremely efficient, future studies could apply it to daily or even hourly sea ice concentration data, allowing for more precise tracking of polynya dynamics over time. This would not only improve detection in seasons or regions where polynyas are small or short-lived, but also open opportunities for large-scale, long-term monitoring of polynya behaviour under different climate conditions. The inclusion of preliminary daily-scale analysis (Fig. 7c) demonstrates this capability in practice. By applying the optimised geomorphon 575 parameters to a full year of daily sea ice concentration data for the Amundsen Sea, the method resolved rapid changes in polynya area that are typically smoothed out in monthly datasets. This result provides clear evidence that the algorithm can handle large spatiotemporal datasets efficiently, overcoming one of the key limitations of existing threshold-based approaches. The ability to process continuous, fine-temporal-resolution data opens new opportunities to quantify short-lived polynya events and examine their variability under different atmospheric and oceanic forcing conditions, which has not been feasible using 580 conventional methods. For example, daily time series derived from the geomorphon method could be used to link short-term polynya openings with synoptic weather systems or atmospheric pressure anomalies, offering new insights into the drivers of variability. Similarly, applying the algorithm to multi-decadal datasets would allow trends in polynya recurrence, duration, and morphology to be tracked consistently through time, supporting climate-scale analyses of changing sea-ice dynamics.

585 The adaptability of the geomorphon algorithm makes it a highly beneficial method for polynya identification. Being able to adjust the parameters enables the user to identify polynyas on a scale which is relevant to the research question and study area. While the moderate search radius used in this study yielded strong results, especially under contemporary conditions, it is important to recognise that polynya size and morphology can change significantly over decadal timescales (Preußer et al., 2015; Park et al., 2018). For example, the Weddell Sea polynya was substantially larger in the 1970s compared to its 2017 590 recurrence, reaching up to 300,000 km^2 (Carsey, 1980; Campbell et al., 2019). In such cases, parameters optimised for contemporary polynyas may require adjustment to remain effective under different climatic regimes. This highlights the need for a flexible framework that allows for parameter re-evaluation when applying the method to historical datasets or projections under future climate scenarios. The geomorphon algorithm provides a novel alternative to traditional sea ice concentration threshold methods, which often rely on fixed spatial or temporal criteria and may not fully capture the dynamic nature of 595 polynya formation and variability. By incorporating surface morphology and adapting to spatial context, the geomorphon approach provides a more nuanced and scalable tool for identifying polynyas across a range of conditions, regions, and time periods.

Beyond statistical comparison, it is also valuable to visually assess how well the geomorphon-detected polynyas correspond 600 to observed features. Figure 8 presents a direct comparison between true-colour satellite imagery of the Amundsen Sea (right panels) and the corresponding geomorphon-detected polynyas (left panels) for 01 December 2020 and 01 December 2001. The spatial correspondence between open-water areas visible in the satellite imagery and those identified by the algorithm confirms that the geomorphon method captures realistic polynya morphology without reliance on predefined thresholds. There are some

https://doi.org/10.5194/egusphere-2026-1653
Preprint. Discussion started: 26 March 2026

minor differences between the satellite and algorithm outputs (for example, slight variations in polynya shape or extent), but these are expected because the satellite imagery represents a single moment in time, whereas the sea-ice concentration data used for the geomorphon analysis are averaged over the entire day. Overall, the strong spatial agreement demonstrates that the algorithm successfully resolves the fine-scale geometry of polynyas observed in satellite imagery, further validating its performance as an automated, morphology-based detection tool.

An additional advantage highlighted by this study is the transferability of the geomorphon method across independent sea ice concentration datasets. Analytical rescaling of parameters enabled successful application to a higher-resolution AMSR2 passive microwave product without further sensitivity testing or empirical tuning. Because each parameter retains a direct physical interpretation, relating to concentration gradients, lookup distance, and maximum detectable landform scale, adjustments required to accommodate differing spatial resolutions are transparent and reproducible. This contrasts with many threshold-based and machine-learning approaches, which frequently require region-specific calibration, labelled training datasets, or retraining when transferred between sensors or environmental conditions (Willmes et al., 2014; Heuzé and Wong, 2025). The ability to transfer parameters between datasets suggests that the geomorphon approach could support multi-decadal analyses combining multiple satellite products or facilitate direct comparison between observational records and climate model output.

https://doi.org/10.5194/egusphere-2026-1653
Preprint. Discussion started: 26 March 2026

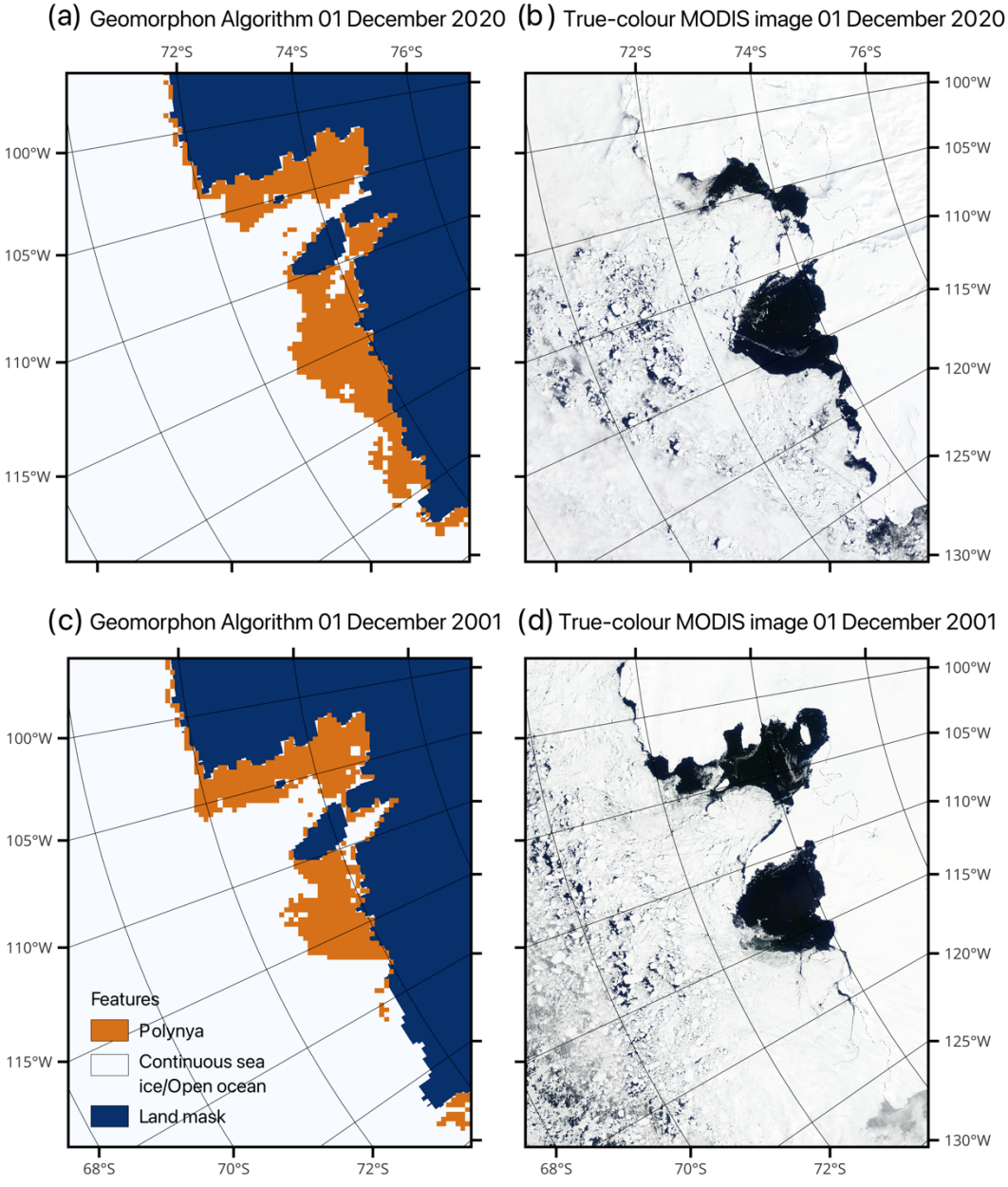

Figure 8: Comparison between geomorphon-detected polynyas (panels a and c) and true-colour satellite imagery (panels b and d) of the Amundsen Sea for (top) 01 December 2020 and (bottom) 01 December 2001. The geomorphon classifications show areas identified as polynyas (orange) relative to continuous sea ice/open ocean (light grey), and land (dark blue). MODIS true-colour imagery from NASA's Level-1 and Atmosphere Archive and Distribution System (LAADS) Distributed Active Archive Center (DAAC) (500 meter MODIS Level-1B MOD02HKM product).

https://doi.org/10.5194/egusphere-2026-1653
Preprint. Discussion started: 26 March 2026

5 Conclusions

This study demonstrates the value of applying the geomorphon algorithm to sea ice concentration data as a novel, automated approach for identifying polynyas. Traditionally, polynya detection has relied on static sea ice concentration thresholds (Kern et al., 2007; Nakata et al., 2015; Ohshima et al., 2016), which can miss features that vary in space and time or fall below arbitrary cut-offs (Massom et al., 1998; Mohrmann et al., 2021). By contrast, although originally developed for terrestrial applications, the geomorphon method can be used to capture spatial structure and morphology directly from sea ice concentration patterns, offering an effective automated detection method. The algorithm's ability to detect polynyas across a wide range of spatial scales, particularly in challenging conditions such as the austral winter, highlights its potential to improve our understanding of when and where open water areas occur.

The automation and flexibility of this method makes it particularly well-suited for investigating long-term dynamics. Because the algorithm does not rely on predefined thresholds, it can be applied across different regions and time periods with minimal manual intervention. Furthermore, the successful transfer of analytically rescaled parameters to an independent sea ice concentration dataset demonstrates that the geomorphon framework is not intrinsically tied to a single dataset or spatial resolution. These features of the method create the potential for long-term and large-scale detection of polynyas, which could provide vital information for understanding potential changes to their role in climate patterns and ocean circulation (Melling et al., 2001; Hoppema and Anderson, 2007). The ability to map polynya extent and structure with greater reliability also has important implications for top predator ecology (Gilchrist and Robertson, 2000; Labrousse et al., 2018), primary productivity (Arrigo and van Dijken, 2003; Arrigo et al., 2008), and conservation planning (Boothroyd et al., 2024), particularly in the rapidly changing polar oceans.

Our study highlights an avenue for future research to apply the geomorphon algorithm to daily-resolution sea ice concentration data. The efficiency of the geomorphon algorithm, combined with its capacity for automation, means that running the method on daily datasets is now a feasible next step. Doing so would allow for more accurate detection of polynya dynamics and improve the temporal precision of analyses. In addition, there is scope to integrate this approach with climate model output to assess future changes in polynya distribution under different warming scenarios. As sea ice conditions shift, being able to detect and compare polynya features across both observational and modelled datasets will be key to understanding their role in ecosystem resilience and ocean-atmosphere interactions.

https://doi.org/10.5194/egusphere-2026-1653
Preprint. Discussion started: 26 March 2026

Appendices

Appendix A: Geomorphon landforms assigned to areas classified as polynyas and non-polynyas by the threshold-based method

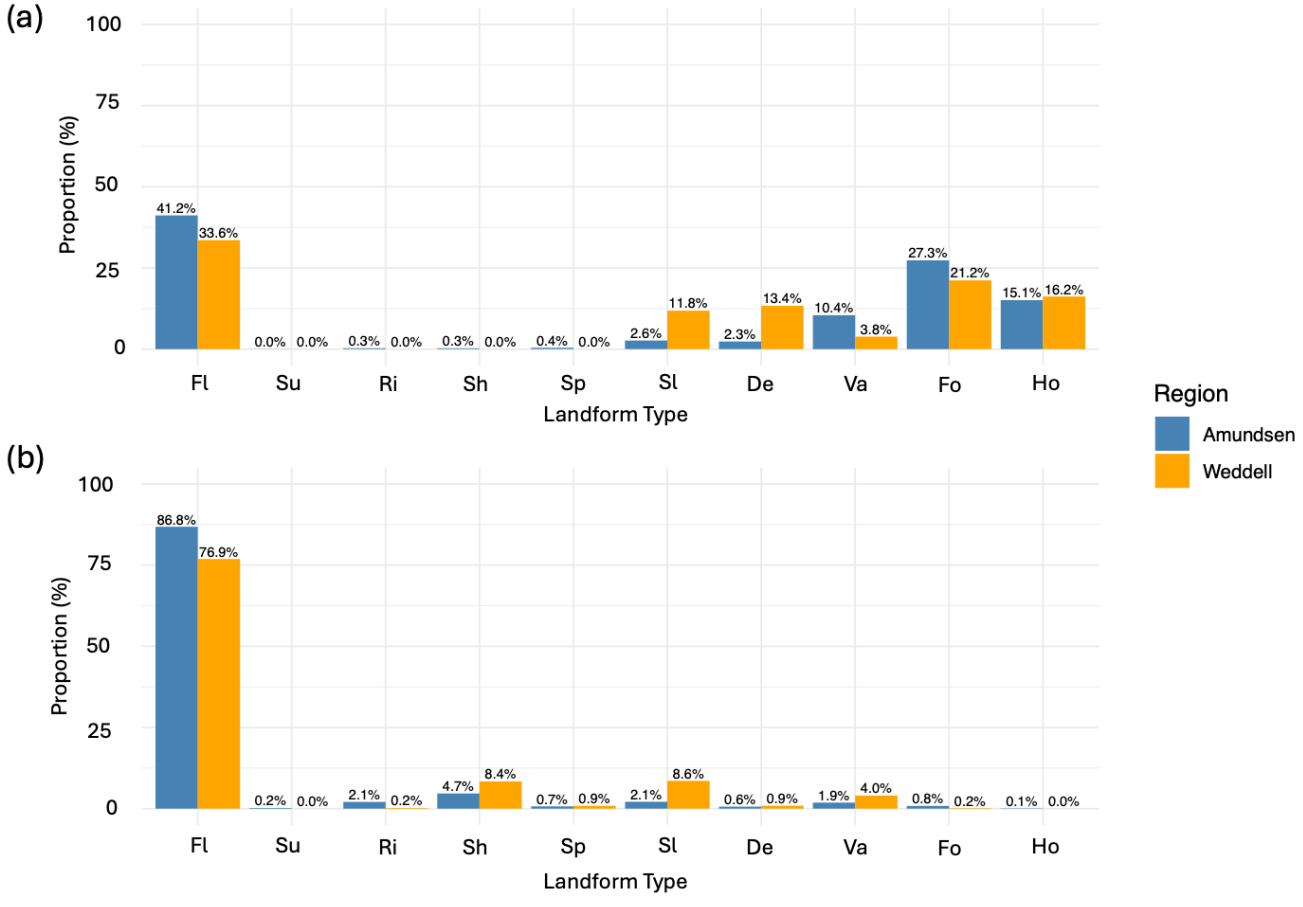

Figure A1: The proportion of geomorphon landforms (Fig. 2) assigned to (a) polynya and (b) non-polynya areas, defined by the sea ice concentration threshold-based method, across all tested parameter combinations for both regions.

https://doi.org/10.5194/egusphere-2026-1653
Preprint. Discussion started: 26 March 2026

Appendix B: Precision and recall scores for geomorphon algorithm when compared to threshold-based method

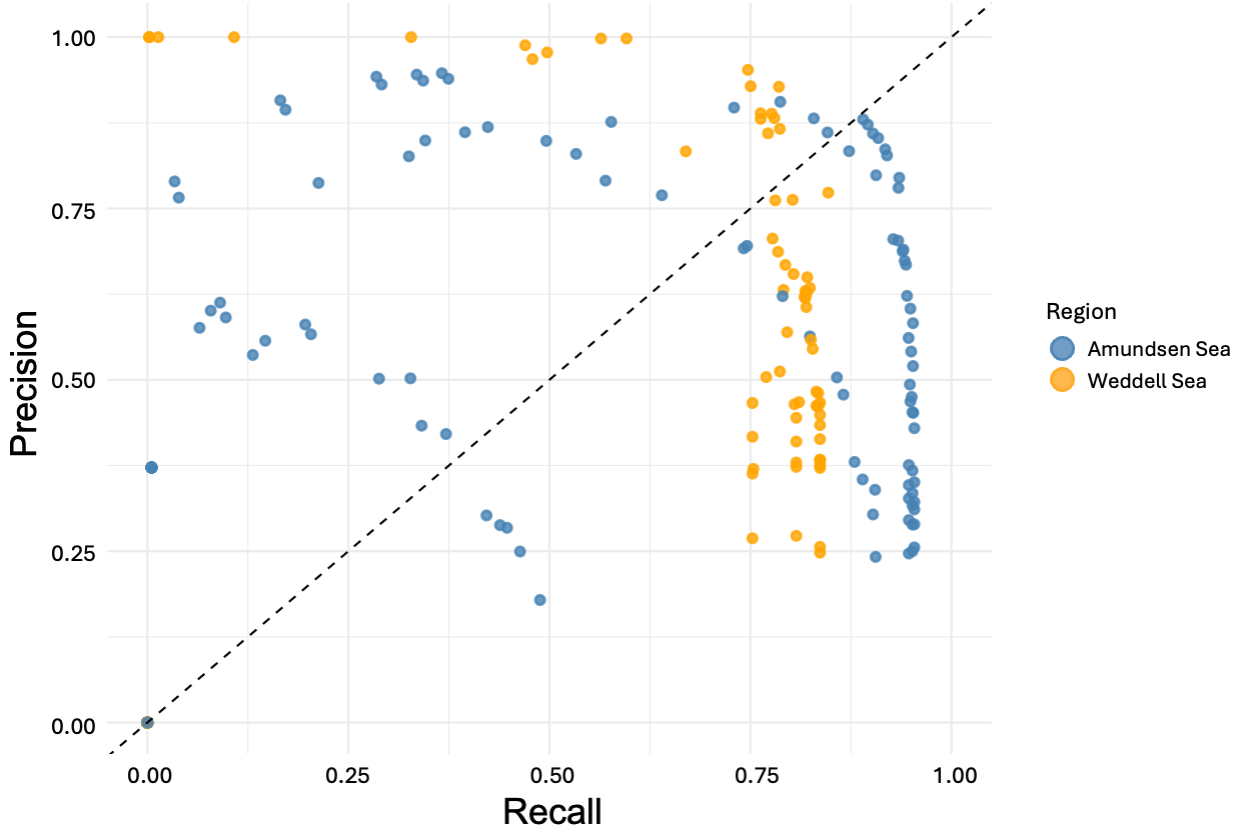

Figure B1: Precision-recall plot comparing the performance of the geomorphon algorithm across parameter combinations for the Amundsen (blue) and Weddell (orange) Seas. Each point represents a unique parameter configuration, evaluated by its precision and recall scores based on comparison to polynyas defined by the sea ice concentration method. The dashed diagonal line indicates equal precision and recall. Points closer to this line represent balanced performance, while deviations suggest a trade-off between the two metrics.

https://doi.org/10.5194/egusphere-2026-1653
Preprint. Discussion started: 26 March 2026

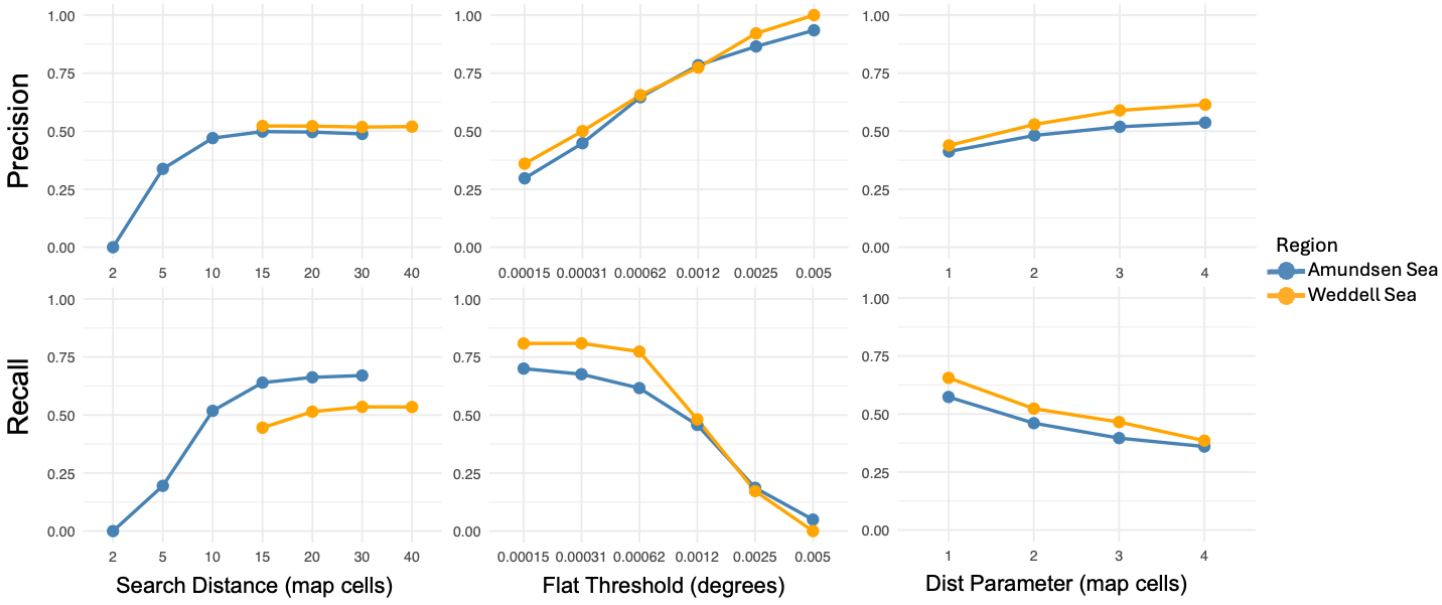

Figure B2: Precision (top row) and recall (bottom row) scores for different parameter values (*search*, *flat*, *dist*) used in iterations of the geomorphon algorithm in the Amundsen (blue) and Weddell (orange) Seas. Precision and recall scores are calculated as averages for each parameter value, considering its combination with all values from the other two parameters in each iteration.

https://doi.org/10.5194/egusphere-2026-1653
Preprint. Discussion started: 26 March 2026

Appendix C: Transferability of geomorphon-derived polynya detection across independent sea ice concentration datasets

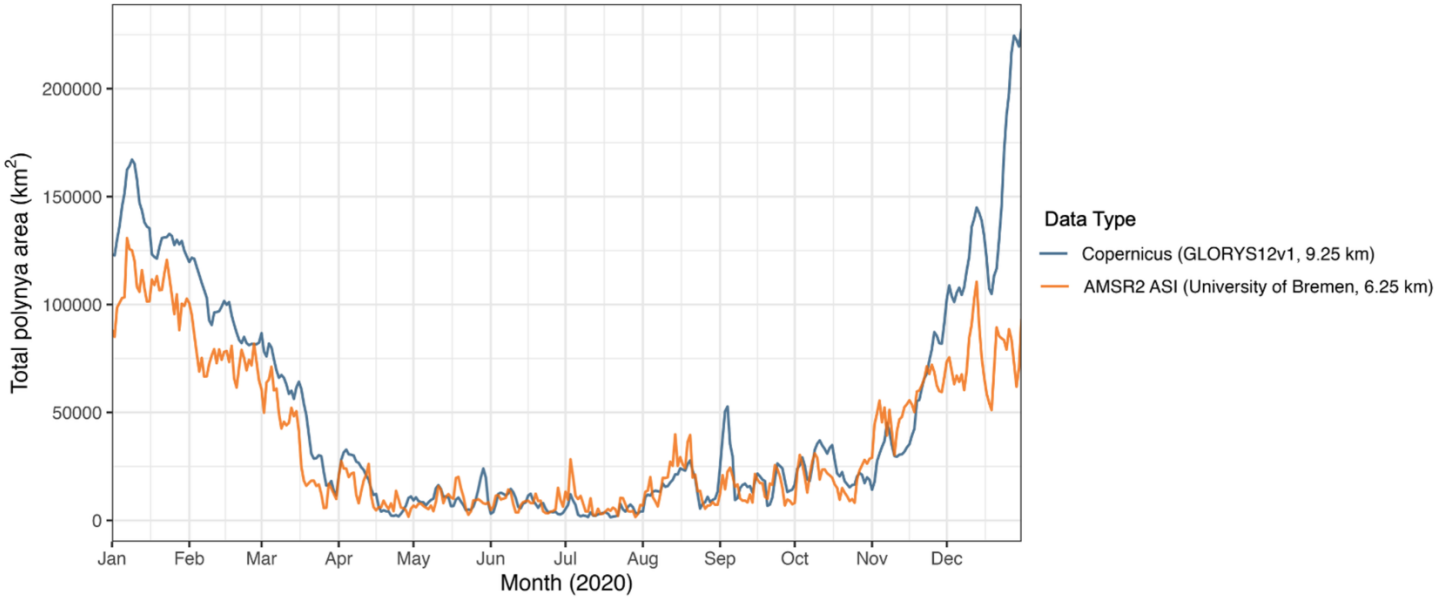

Figure C1: Comparison of daily total polynya area within the Amundsen Sea derived using geomorphon classification applied to Copernicus (GLORYS12v1, 9.25 km resolution) (blue) and independently rescaled AMSR2 ASI (University of Bremen, 6.25 km resolution) (orange) sea ice concentration datasets during 2020. Parameters applied to the AMSR2 dataset were analytically rescaled to preserve equivalent physical interpretations of concentration gradient threshold, lookup distance, and maximum detectable landform size.

Code and data availability

The geomorphon algorithm code used in this study is available at https://github.com/miahurst/geomorphon_method_polynyas. Data can be accessed through the Copernicus Marine Data Store (Lellouche et al. 2021) (https://doi.org/10.3389/feart.2021.698876) and PANGAEA Data Publisher for Earth & Environmental Science (Melsheimer and Spreen, 2019) (https://doi.org/10.1594/PANGAEA.898400).

Author contributions

MH conceptualised research idea; formal analysis undertaken by MH; methodology designed by MH and LB; supervision carried out by LB; visualisation and writing (original draft preparation) by MH; writing (review and editing) MH and LB.

https://doi.org/10.5194/egusphere-2026-1653
Preprint. Discussion started: 26 March 2026

Competing interests

The authors declare that they have no conflict of interest.

Financial support

This work was supported by the Drivers of Oceanic Change in the Amundsen Sea (DeCAdeS) under Grant Number NE/T012773/1.

References

Alam, A. and Curry, J.: (1995). Lead-induced atmospheric circulations, J. Geophys. Res.-Oceans, 100, 4643-4651, https://doi.org/10.1029/94JC02562, 1995.

Albaji, A. O., Rashid, R. B. A. and Hamid, S. Z. A.: Investigation on Machine Learning Approaches for Environmental Noise Classifications, Ele. Com. Eng., 3615137, 1-26, https://doi.org/10.1155/2023/3615137, 2022.

Alem, A. and Kumar, S.: Deep Learning Models Performance Evaluations for Remote Sensed Image Classification, IEEE Access, 10, 111784-111793, https://doi.org/10.1109/ACCESS.2022.3215264, 2022.

Andersen, S., Tonboe, R., Kaleschke, L., Heygster, G. and Pedersen, L. T.: Intercomparison of passive microwave sea ice concentration retrievals over the high-concentration Arctic sea ice, J. Geophys. Res.-Oceans, 112, 1-18, https://doi.org/10.1029/2006JC003543, 2007.

Antonello, A., Franceschi, S., Floreancig, V., Comiti, F. and Tonon, G.: Application of a Pattern Recognition Algorithm for Single Tree Detection from Lidar Data, Int. Arch. Photogramm., XLII-4/W2, 27-33, https://doi.org/10.5194/isprs-archives-XLII-4-W2-27-2017, 2017.

Arrigo, K. R. and van Dijken, G. L.: Phytoplankton dynamics within 37 Antarctic coastal polynya systems, J. Geophys. Res.-Oceans, 108, 1-18, https://doi.org/10.1029/2002JC001739, 2003.

Arrigo, K. R., van Dijken, G. L. and Bushinsky, S.: Primary production in the Southern Ocean, 1997-2006, J. Geophys. Res.-Oceans, 113, 1-27, https://doi.org/10.1029/2007JC004551, 2008.

https://doi.org/10.5194/egusphere-2026-1653
Preprint. Discussion started: 26 March 2026

765 Arrigo, K., Lowry, K. and van Dijken, G.: Annual changes in sea ice and phytoplankton in polynyas of the Amundsen Sea, Antarctica, Deep-Sea Res. Pt. II, 71-76, 5-15, https://doi.org/10.1016/j.dsr2.2012.03.006, 2012.

Barber, D. G. and Massom, R. A.: The Role of Sea Ice in Arctic and Antarctic Polynyas, in: Polynyas - Windows to the World, edited by: Smith, W. O. and Barber, D. G., Elsevier Oceanography Series, 1-54, https://doi.org/10.1016/S0422-
770 9894(06)74001-6, 2007.

Barber, D., Marsden, R., Minnett, P., Ingram, G. and Fortier, L.: Physical processes within the North Water (NOW) polynya, Atmos.-Ocean, 39(3), 163-166, https://doi.org/10.1080/07055900.2001.9649673, 2001.

775 Behera, B., Kumaravelan, G. and Kumar, P. B.: Performance Evaluation of Deep Learning Algorithms in Biomedical Document Classification, 11th Int. Conf. Adv. Comput. (ICoAC), Chennai, India, 220-224, https://doi.org/10.1109/ICoAC48765.2019.246843, 2019.

Bennett, M., Renfrew, I., Stevens, D. and Moore, G.: The Northeast Water Polynya, Greenland: Climatology, Atmospheric
780 Forcing and Ocean Response, J. Geophys. Res.-Oceans, 129(5), 1-24, https://doi.org/10.1029/2023JC020513, 2024.

Bitz, C. M., Holland, M. M., Hunke, E. C. and Moritz, R. E.: Maintenance of the Sea-Ice Edge, J. Climate, 18(15), 2903-2921, https://doi.org/10.1175/JCLI3428.1, 2005.

785 Boothroyd, A., Adams, V., Alexander, K. and Hill, N.: Priority areas for marine protection in the Amundsen and Bellingshausen Seas, Antarctica, Mar. Policy, 167(106232), 1-11, https://doi.org/10.1016/j.marpol.2024.106232, 2024.

Bromwich, D. H. and Kurtz, D. D.: Katabatic wind forcing of the Terra Nova Bay polynya, J. Geophys. Res., 89, 3561-3572, https://doi.org/10.1029/JC089iC03p03561, 1984.

790

Budikova, D.: Role of Arctic sea ice in global atmospheric circulation: A review, Global Planet. Change, 68(3), 149-163, https://doi.org/10.1016/j.gloplacha.2009.04.001, 2009.

Burada, G., McDonald, A., Renwick, J. and Jolly, B.: Delineating Polynya Area Using Active and Passive Microwave Sensors
795 for the Western Ross Sea Sector of Antarctica, Remote Sens., 15(10), 1-23, https://doi.org/10.3390/rs15102545, 2023.

https://doi.org/10.5194/egusphere-2026-1653
Preprint. Discussion started: 26 March 2026

Campbell, E. C., Wilson, E. A., Kent Moore, G. W., Rider, S. C., Brayton, C. E., Mazloff, M. R. and Talley, L. D.: Antarctic offshore polynyas linked to Southern Hemisphere climate anomalies, Nature, 570, 319-325, https://doi.org/10.1038/s41586-019-1294-0, 2019.

Carsey, F. D.: Microwave Observation of the Weddell Sea Polynya, Mon. Weather Rev., 108(12), 2032-2044, https://doi.org/10.1175/1520-0493(1980)108%3C2032:MOOTWP%3E2.0.CO;2, 1980.

Cheon, W. G. and Gordon, A.: Open-ocean polynyas and deep convection in the Southern Ocean, Sci. Rep., 9(6935), https://doi.org/10.1038/s41598-019-43466-2, 2019.

Chorowicz, J., Parrot, J.-F., Taud, H., Hakdaoui, M., Rudant, J. P. and Rois, T.: Automated pattern-recognition of geomorphic features from DEMs and satellite images, Z. Geomorphol. Suppl., 101, 69-84, 1995.

Comiso, J. and Gordon, A.: Interannual Variability in Summer Sea Ice Minimum, Coastal Polynyas and Bottom Water Formation in the Weddell Sea, in: Antarctic Sea Ice: Physical Processes, Interactions and Variability, 74, 293-315, https://doi.org/10.1029/AR074p0293, 1998.

Comiso, J. C., Cavalieri, D. J. and Markus, T.: Sea ice concentration, ice temperature, and snow depth using AMSR-E data, IEEE T. Geosci. Remote, 41, 243-252, https://doi.org/10.1109/TGRS.2002.808317, 2003.

Cook, J. and Ramadas, V.: When to consult precision-recall curves, Stata J., 20, 131-148, https://doi.org/10.1177/1536867X20909693, 2020.

Dennett, M., Mathot, S., Caron, D., Smith Jr, W. and Lonsdale, D.: Abundance and distribution of phototrophic and heterotrophic nano- and microplankton in the southern Ross Sea, Deep-Sea Res. Pt. II, 48, 4019-4037, https://doi.org/10.1016/S0967-0645(01)00079-0, 2001.

Else, B. G. T., Papakyriakou, T. N., Asplin, M. G., Barber, D. G., Galley, R. J., Miller, L. A. and Mucci, A.: Annual cycle of air-sea CO_2 exchange in an Arctic Polynya Region, Global Biogeochem. Cy., 27, 388-398, https://doi.org/10.1002/gbc.20016, 2013.

Flynn, T., Rozanov, A., Ellis, F., de Clercq, W. and Clarke, C.: Farm-scale soil patterns derived from automated terrain classification, Catena, 185, 1-11, https://doi.org/10.1016/j.catena.2019.104311, 2020.

https://doi.org/10.5194/egusphere-2026-1653
Preprint. Discussion started: 26 March 2026

Fu, H., Zhao, J. and Frey, K. E.: Investigation of polynya dynamics in the northern Bering Sea using greyscale morphology image-processing techniques, Int. J. Remote Sens., 33, 2214-2232, https://doi.org/10.1080/01431161.2011.608088, 2011.

Gallée, H.: Air-sea interactions over Terra Nova Bay during winter: Simulation with a coupled atmosphere-polynya model, J. Geophys. Res.-Atmos., 102, 13835-13849, https://doi.org/10.1029/96JD03098, 1997.

Gilchrist, G. and Robertson, G.: Observations of Marine Birds and Mammals Wintering at Polynyas and Ice Edges in the Belcher Islands, Nunavut, Canada, Arctic, 53, 61-68, https://doi.org/10.14430/arctic835, 2000.

Gordon, A. L. and Comiso, J. C.: Polynyas in the Southern Ocean, Sci. Am., 258, 90-97, http://dx.doi.org/10.1038/scientificamerican0688-90, 1988.

Gutjahr, O., Heinemann, G., Preußer, A., Willmes, S. and Drüe, C.: Quantification of ice production in Laptev Sea polynyas and its sensitivity to thin-ice parameterizations in a regional climate model, The Cryosphere, 10, 2999-3019, https://doi.org/10.5194/tc-10-2999-2016, 2016.

Hall, D., Key, J., Casey, K., Riggs, G. and Cavalieri, D.: Sea Ice Surface Temperature Product From MODIS, IEEE T. Geosci. Remote, 42, 1076-1087, https://doi.org/10.1109/TGRS.2004.825587, 2004.

Holz, R., Ackerman, S., Nagle, F., Frey, R., Dutcher, S., Kuehn, R., Vaughan, M. and Baum, B.: Global Moderate Resolution Imaging Spectroradiometer (MODIS) cloud detection and height evaluation using CALIOP, J. Geophys. Res.-Atmos., 113, 1-17, https://doi.org/10.1029/2008JD009837, 2008.

Hoppema, M. and Anderson, L.: Biogeochemistry of polynyas and their role in sequestration of anthropogenic constituents, in: Polynyas - Windows to the World, edited by: Smith, W. O. and Barber, D. G., chap. Biogeochemistry of polynyas and their role in sequestration of anthropogenic constituents, 193-221, Elsevier Oceanography Series, https://doi.org/10.1016/S0422-9894(06)74006-5, 2007.

Houghton, J., Filho, L. M., Callander, B., Harris, N., Kattenberg, A. and Maskell, K.: Climate Change 1995: The Science of Climate Change: contribution of working group I to the second assessment report of the Intergovernmental Panel on Climate Change, 2, Cambridge University Press, https://www.ipcc.ch/site/assets/uploads/2018/02/ipcc_sar_wg_I_full_report.pdf, 1996.

https://doi.org/10.5194/egusphere-2026-1653
Preprint. Discussion started: 26 March 2026

Heuzé, C., and Wong, W.: Automatic detection of Arctic polynyas using hybrid supervised-unsupervised deep learning, EGUsphere [preprint], https://doi.org/10.5194/egusphere-2025-2747, 23 June 2025.

Heuzé, C., Zhou, L., Mohrmann, M., and Lemos, A.: Spaceborne infrared imagery for early detection of Weddell Polynya opening, The Cryosphere, 15, 3401-3421, https://doi.org/10.5194/tc-15-3401-2021, 2021.

Iwamoto, K., Ohshima, K. I. and Tamura, T.: Improved mapping of sea ice production in the Arctic Ocean using AMSR-E thin ice thickness algorithm, 119, 3574-3594, https://doi.org/10.1002/2013JC009749, 2014.

Jasiewicz, J. and Stepinski, T. F.: Geomorphons - a pattern recognition approach to classification and mapping of landforms, Geomorphology, 182, 147-156, http://dx.doi.org/10.1016/j.geomorph.2012.11.005, 2013.

Jena, B. and Pillai, A.: Satellite observations of unprecedented phytoplankton blooms in the Maud Rise polynya, Southern Ocean, The Cryosphere, 14, 1385-1398, https://doi.org/10.5194/tc-14-1385-2020, 2020.

Jena, B., Ravichandran, M. and Turner, J.: Recent reoccurrence of large open-ocean polynya on the Maud Rise Seamount, Geophys. Res. Lett., 46, 4320-4329, https://doi.org/10.1029/2018GL081482, 2019.

Jiang, L., Ma, Y., Chen, F., Liu, J., Yao, W., Qiu, Y. and Zhang, S.: Trends in the stability of Antarctic coastal polynyas and the role of topographic forcing factors, Remote Sens., 12, 1-21, https://doi.org/10.3390/rs12061043, 2020.

Kern, S., Spreen, G., Kaleschke, L., De La Rosa, S. and Heygster, G.: Polynya Signature Simulation Method polynya area in comparison to AMSR-E 89 GHz sea-ice concentrations in the Ross Sea and off the Adélie Coast, Antarctica, for 2002-05: first results, Ann. Glaciol., 46, 410-418, https://doi.org/10.3189/172756407782871585, 2007.

Kim, Y., Min, S., Gillett, N., Notz, D. and Malinina, E.: Observationally-constrained projections of an ice-free Arctic even under a low emission scenario, Nat. Commun., 14, 3139, https://doi.org/10.1038/s41467-023-38511-8, 2023.

Kimura, N. and Wakatsuchi, M.: Increase and decrease of sea ice area in the Sea of Okhotsk: Ice production in coastal polynyas and dynamic thickening in convergence zones, J. Geophys. Res.-Oceans, 109, C09S03, https://doi.org/10.1029/2003JC001901, 2004.

Kwok, R., Comiso, J. C., Martin, S. and Drucker, R.: Ross Sea polynyas: Response of ice concentration retrievals to large areas of thin ice, J. Geophys. Res.-Oceans, 112, 1-13, https://doi.org/10.1029/2006JC003967, 2007.

https://doi.org/10.5194/egusphere-2026-1653
Preprint. Discussion started: 26 March 2026

Labrousse, S., Williams, G., Tamura, T., Bestley, S., Sallée, J., Fraser, A., Sumner, M., Roquet, F., Heerah, K., Picard, B., Guinet, C., Harcourt, R., McMahon, C., Hindell, M. and Charrassin, J.: Coastal polynyas: Winter oases for subadult southern elephant seals in East Antarctica, Sci. Rep., 8, 3183, https://doi.org/10.1038/s41598-018-21388-9, 2018.

Landrum, L. L. and Holland, M. M.: Influences of changing sea ice and snow thickness on simulated Arctic winter heat fluxes, The Cryosphere, 16, 1483-1495, https://doi.org/10.5194/tc-16-1483-2022, 2022.

Lee, Y., Park, J., Jung, J. and Wan Kim, T.: Unprecedented differences in phytoplankton community structures in the Amundsen Sea polynyas, West Antarctica, Environ. Res. Lett., 17, 1-8, https://doi.org/10.1088/1748-9326/ac9a5f, 2022.

Lellouche, J.-M., Greiner, E., Bourdallé-Badie, R., Garric, G., Melet, A., Drévillon, M., Bricaud, C., Hamon, M., Le Galloudec, O., Regnier, C., Candela, T., Testut, C.-E., Gasparin, F., Ruggiero, G., Benkiran, M., Drillet, Y., and Le Traon, P.-Y.: The Copernicus global 1/12° oceanic and sea ice GLORYS12 reanalysis, Front. Earth Sci., 9, 698876, https://doi.org/10.3389/feart.2021.698876, 2021.

Louanchi, F., Hoppema, M., Bakker, D. C. E., Poisson, A., Stoll, M. H. C., De Baar, H. J. W., Schauer, B., Ruiz-Pino, D. P., and Wolf-Gladrow, D.: Modelled and observed sea surface fCO_2 in the Southern Ocean: a comparative study, Tellus B, 51, 541-559, https://doi.org/10.1034/j.1600-0889.1999.00029.x, 1999.

Macdonald, G. J., Ackley, S. F., Mestas-Nuñez, A. M., and Blanco-Cabanillas, A.: Evolution of the dynamics, area, and ice production of the Amundsen Sea Polynya, Antarctica, 2016-2021, The Cryosphere, 17, 457-476, https://doi.org/10.5194/tc-17-457-2023, 2023.

Madec, G. and the NEMO System Team: NEMO Ocean Engine Reference Manual, Zenodo, https://doi.org/10.5281/zenodo.1464816, 2024.

Martinson, D. G.: Open Ocean Convection in the Southern Ocean, in: Elsevier Oceanography Series, 57, 37-52, https://doi.org/10.1016/S0422-9894(08)70059-X, 1991.

Massom, R. A., Harris, P. T., Michael, K. J., and Potter, M. J.: The distribution and formative processes of latent-heat polynyas in East Antarctica, Ann. Glaciol., 27, 420-426, https://doi.org/10.3189/1998AoG27-1-420-426, 1998.

https://doi.org/10.5194/egusphere-2026-1653
Preprint. Discussion started: 26 March 2026

Maykut, G.: Large-scale heat exchange and ice production in the central Arctic, J. Geophys. Res.-Oceans, 87, 7865-8056, https://doi.org/10.1029/JC087iC10p07971, 1982.

Mchedlishvili, A., Spreen, G., Melsheimer, C., and Huntermann, M.: Weddell Sea polynya analysis using SMOS-SMAP apparent sea ice thickness retrieval, The Cryosphere, 16, 471-487, https://doi.org/10.5194/tc-16-471-2022, 2022.

Melling, H., Gratton, Y., and Ingram, G.: Ocean circulation within the North Water Polynya of Baffin Bay, Atmos.-Ocean, 39, 301-325, https://doi.org/10.1080/07055900.2001.9649683, 2001.

Melsheimer, Christian; Spreen, Gunnar.: AMSR2 ASI sea ice concentration data, Antarctic, version 5.4 (NetCDF) (July 2012 - December 2019) [dataset]. PANGAEA, https://doi.org/10.1594/PANGAEA.898400, 2019.

Mohrmann, M., Huezé, C., and Swart, S.: Southern Ocean polynyas in CMIP6 models, The Cryosphere, 15, 4281-4313, https://doi.org/10.5194/tc-15-4281-2021, 2021.

Morales Maqueda, M. A., Willmott, A. J., and Biggs, N. R. T.: Polynya dynamics: a review of observations and modeling, Rev. Geophys., 42, RG1004, https://doi.org/10.1029/2002RG000116, 2004.

Nakata, K., Ohshima, K., Nihashi, S., Kimura, N., and Tamura, T.: Variability and ice production budget in the Ross Ice Shelf Polynya based on a simplified polynya model and satellite observations, J. Geophys. Res.-Oceans, 120, 6234-6252, https://doi.org/10.1002/2015JC010894, 2015.

Neteler, M. and Mitasova, H.: Open Source GIS: A GRASS GIS Approach (3rd Ed.), Springer, New York, https://doi.org/10.1007/978-0-387-68574-8, 2007.

Nomura, D., Abe, H., Hirawake, T., Ooki, A., Yamashita, Y., Murayama, A., Ono, K., and Nishioka, J.: Formation of dense shelf water associated with sea ice freezing in the Gulf of Anadyr estimated with oxygen isotopic ratios, Prog. Oceanogr., 196, 102595, https://doi.org/10.1016/j.pocean.2021.102595, 2021.

Ohshima, K., Nihashi, S., and Iwamoto, K.: Global view of sea-ice production in polynyas and its linkage to dense/bottom water formation, Geosci. Lett., 3, 13, https://doi.org/10.1186/s40562-016-0045-4, 2016.

Park, J., Kim, H.-C., Jo, Y.-H., Kidwell, A., and Hwang, J.: Multi-temporal variation of the Ross Sea Polynya in response to climate forcings, Polar Res., 37, 1444891, https://doi.org/10.1080/17518369.2018.1444891, 2018.

https://doi.org/10.5194/egusphere-2026-1653
Preprint. Discussion started: 26 March 2026

Paul, S., Willmes, S., and Heinemann, G.: Long-term coastal-polynya dynamics in the southern Weddell Sea from MODIS thermal-infrared imagery, The Cryosphere, 9, 2027-2041, https://doi.org/10.5194/tc-9-2027-2015, 2015.

Preußer, A., Heinemann, G., Willmes, S., and Paul, S.: Multi-decadal variability of polynya characteristics and ice production in the North Water Polynya by means of passive microwave and thermal infrared satellite imagery, Remote Sens., 7, 15844-15867, https://doi.org/10.3390/rs71215807, 2015.

Stepinski, T. F. and Jasiewicz, J.: Geomorphons - a new approach to classification of landforms, in: Proc. Geomorphometry 2011, 109-112, 2011.

Stringer, W. J. and Groves, J. E.: Location and areal extent of polynyas in the Bering and Chukchi Seas, Arctic, 44, 164-171, https://doi.org/10.14430/ARCTIC1583, 1991.

Tamura, T. and Ohshima, K. I.: Mapping of sea ice production in the Arctic coastal polynyas, J. Geophys. Res.-Oceans, 116, https://doi.org/10.1029/2010JC006586, 2011.

van Manen, M., Aoki, S., Brussaard, C. P. D., Conway, T. M., Eich, C., Gerringa, L. J. A., Jung, J., Kim, T.-W., Lee, S., Lee, Y., Reichart, G.-J., T., H.-A., Wille, F., and Middag, R.: The role of the Dotson Ice Shelf and Circumpolar Deep Water as driver and source of dissolved and particulate iron and manganese in the Amundsen Sea polynya, Southern Ocean, Mar. Chem., 246, 1-22 https://doi.org/10.1016/j.marchem.2022.104161, 2022.

Wakatsuchi, M., and Ono, N.: Measurements of salinity and volume of brine excluded from growing sea ice, J. Geophys. Res.-Oceans, 88, 2943-2951, https://doi.org/10.1029/JC088iC05p02943, 1983.

Walsh, J. E., and Johnson, C. M.: Interannual atmospheric variability and associated fluctuations in Arctic sea ice extent, J. Geophys. Res.-Oceans, 84, 6915-6928, https://doi.org/10.1029/JC084iC11p06915, 1979.

Wang, X., Zhang, Z., Wang, X., Vihma, T., Zhou, M., Yu, L., Uotila, P., and Sein, D. V.: Impacts of strong wind events on sea ice and water mass properties in Antarctic coastal polynyas, Clim. Dyn., 57, 3505-3528, https://doi.org/10.1007/s00382-021-05878-7, 2021.

Worby, A. P., and Comiso, J. C.: Studies of the Antarctic sea ice edge and ice extent from satellite and ship observations, Remote Sens. Environ., 92, 98-111, https://doi.org/10.1016/j.rse.2004.05.007, 2004.

https://doi.org/10.5194/egusphere-2026-1653
Preprint. Discussion started: 26 March 2026

Wyles, H. M. E., Boehme, L., Russell, D. J. F., and Carter, M. I. D.: A novel approach to using seabed geomorphology as a predictor of habitat use in highly mobile marine predators: Implications for ecology and conservation, Front. Mar. Sci., 9, 1-16, https://doi.org/10.3389/fmars.2022.818635, 2022.

Yager, P. L., Sherrell, R. M., Stammerjohn, S. E., Ducklow, H. W., Schofield, O. M. E., Ingall, E. D., Wilson, S. E., Lowry, K. E., Williams, C. M., Riemann, L., Bertilsson, S., Alderkamp, A.-C., Dinasquet, J., Logares, R., Richert, I., Sipler, R. E., Melara, A. J., Mu, L., Newstead, R. G., Post, A. F., Swalethorp, R., and van Dijken, G. L.: A carbon budget for the Amundsen Sea Polynya, Antarctica: Estimating net community production and export in a highly productive polar ecosystem, Elementa Sci. Anthr., 4, 1-36, https://doi.org/10.12952/journal.elementa.000140, 2016.

Yokoyama, R., Shirasawa, M., and Pike, R. J.: Visualizing topography by openness: A new application of image processing to digital elevation models, Photogramm. Eng. Remote Sens., 68, 257-265, 2002.

Zheng, W., Zhaoru, Z., Vihma, T., Xiaoqiao, W., and Yuanjie, C.: An overview of Antarctic polynyas: Sea ice production, forcing mechanisms, temporal variability and water mass formation, Adv. Polar Sci., 32, 295-311, https://doi.org/10.13679/j.advps.2021.0026, 2021.

Zhou, L., Heuzé, C., and Mohrmann, M.: Sea ice production in the 2016 and 2017 Maud Rise polynyas, J. Geophys. Res.-Oceans, 128, 1-20, https://doi.org/10.1029/2022JC019148, 2023.